Final report

1. Project details

Project title	Exhaust gas valve for high temperatures in two-stroke ship engines
Project identification (program abbrev. and file)	64014-0545
Name of the programme which has funded the project	EUDP 14-II, Energieffektivitet
Project managing company/institution (name and address)	MAN Diesel & Turbo, Filial af MAN Diesel & Turbo SE, Tyskland Teglholmsgade 41 2450 København SV
Project partners	Sandvik Powder Solutions AB (SPS) DTU Mekanik (DTU)
CVR (central business register)	31611792
Date for submission	2018-01-31

2. Short description of project objective and results

The overall project objective is to develop a high temperature exhaust valve spindle in a 2-stroke marine diesel engine, which permits high efficiency process modes in order to lower fuel consumption and CO_2 emission.
The spindle is to be produced of a compound spindle disc incorporating Powder Metallurgical (P/M) disc coatings to counteract the specific loads as well as a hollow stem which is friction welded to the spindle disc.
In the project advanced production methods for the compound disc have been developed however without fully meeting the material specifications. A simulation tool for the mechanical service performance of the compound design is developed. Further the process parameters of the friction welding and an advanced simulation tool for the friction welding have been developed.
The base material and basic coatings for the disc and stem are identified however the final compound design including buffer layer between the base material and coatings needs to be developed. Moreover the verification of the mechanical properties and service performance of the compound disc is missing.

Projektets overordnede opgave er at udvikle en højtemperatur bestandig udstødsventil spindel til en 2-takts marine diesel motor som muliggør anvendelsen af motorprocesser som sikrer høj effektivitet med henblik for at reducere brændstof forbruget og dermed nedsat CO_2 emission.
Ventilspindlen søges at blive produceret som en kompound tallerken som omfatter pulvermetallurgisk (P/M) bundne belægninger som er udvalgt til at modstå de forskellige påvirkninger. Den færdige ventilspindel består af en kompoundtallerken og et rørformet skaft som er forbundet via en friktionssvejsning.
I projektets forløb er udviklet avancerede produktionsmetoder for fremstillingen af kompoundtallerknen dog uden at opnå den ønskede materialekvalitet. Avancerede simuleringsværktøjer er udviklet for at analysere påvirkninger i drift. Endvidere er procesparametrene

for friktionssvejsningen identificeret og et nyt simuleringsværktøj for svejsninger er udviklet og verificeret.
Grundmaterialet og de væsentlige coatings er bestemt, men det endelige tallerkendesign og bufferlaget mellem grundmaterialet og belægningerne udestår at blive identificeret. Desuden mangler verifikationen af de mekaniske egenskaber samt driftsperformance af den endelige kompound tallerken.

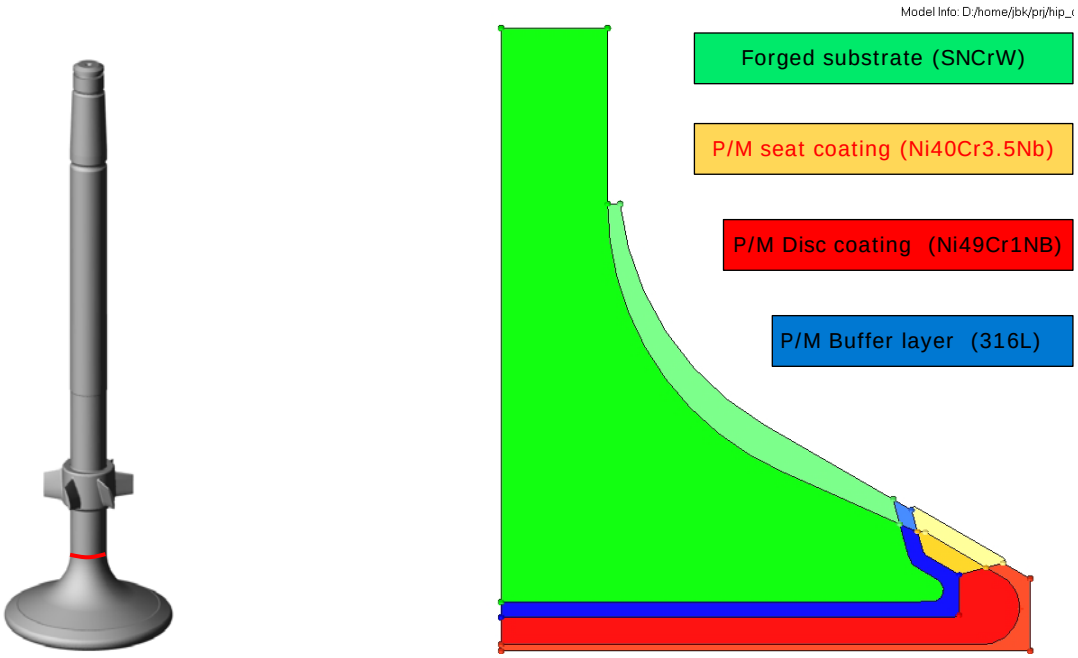

Figure 1 Friction welded spindle and HIP compound capsule elements

3. Executive summary

The background for the set-up of the present project can be summarised in the below bullet points.

- A strong need for a heavy duty exhaust valve spindle to counteract increased heat load in present and future high efficiency 2-stroke marine diesel engines
- Maintaining a high service reliability and service interval of the exhaust valve hereby strengthening MDT's position as a competitive engine supplier
- Co-operating with SPS as a strong partner within development and production of P/M HIP products to mature the HIP production technology
- Co-operation with DTU with the purpose to develop the friction welding process for assembling the spindle disc with the spindle stem
- Applying the MDT CPH production business unit to mature and implement the new product in the spare part and component portfolio as a standard/alternative execution

Previous research has revealed that a compound spindle produced from high Cr bearing Ni-alloy P/M HIP coatings is the answer to the project objective; however unexpected plastic deformation of the compound design was experienced during service. In the present project the object is to develop a sound compound design, with prolonged and stable service performance and not at least reduced production cost.

The task of simulating and verifying the performance of the compound design at MDT experienced a substantial delay due to initial challenges with continued disagreements between calculations and test results, as well as the subsequent unexpected need for costly and time consuming material data. Only at the end of the project the simulation model was completed.

In order to accomplish necessary reductions in the production cost, 3-D printing of details of the compound assembly was pursued by SPS. Promising technologies were developed, however continued and unexpected difficulties in obtaining the required low oxygen level in the parts were the reason for not being able to fulfil the task within the timeframe of the project. The development of a wear resistant P/M seat coating likewise proved to be a challenging task not being able to identify useful dry lubricant additives within the project.

The initial set up of geometry and friction welding method proved to be a success with an unexpected wide process window. Also development of the simulation tool at DTU and its validation was completed successfully on schedule.

Since the project objective is not fulfilled the next step is on the basis of the present results to estimate the extent of efforts required to solve the open issues. Also since the MDT production business unit in the meantime decided to shut down its valve spindle production, it will be necessary with present data at hand, under the changed market conditions, to evaluate the competitiveness of the HIP compound spindle towards other newly developed solutions.

4. Project objectives

The main project objectives were to develop a compound spindle disc produced by the Hot Isostatic Pressure (HIP) process involving a substrate, custom coatings and an intermediate buffer layer which demonstrates superior corrosion resistance and negligible deformation during the entire service life. In order to reduce production cost and reduce the component weight the process parameters for friction welding a hollow spindle stem to the spindle disc had to be developed as well as new production methods for 3-D printed and sintered powder inserts in the compound capsule had to be identified.
Once all production parameters and details were defined a number of prototype spindles had to be produced for verification of the process parameters and for a service test on a commercial vessel.
To fulfil the above objectives the project was divided into the below Work Packages

WP1 Project management and reporting
WP2 HIP spindle geometry changes
WP3 Friction welding
WP4 Development of a dry lubricating spindle material
WP5 Application of additive manufacturing to valve production
WP6 Service test of 60 ME and 90 ME valve spindles

Including the initial project schedule shown in Figure 2.

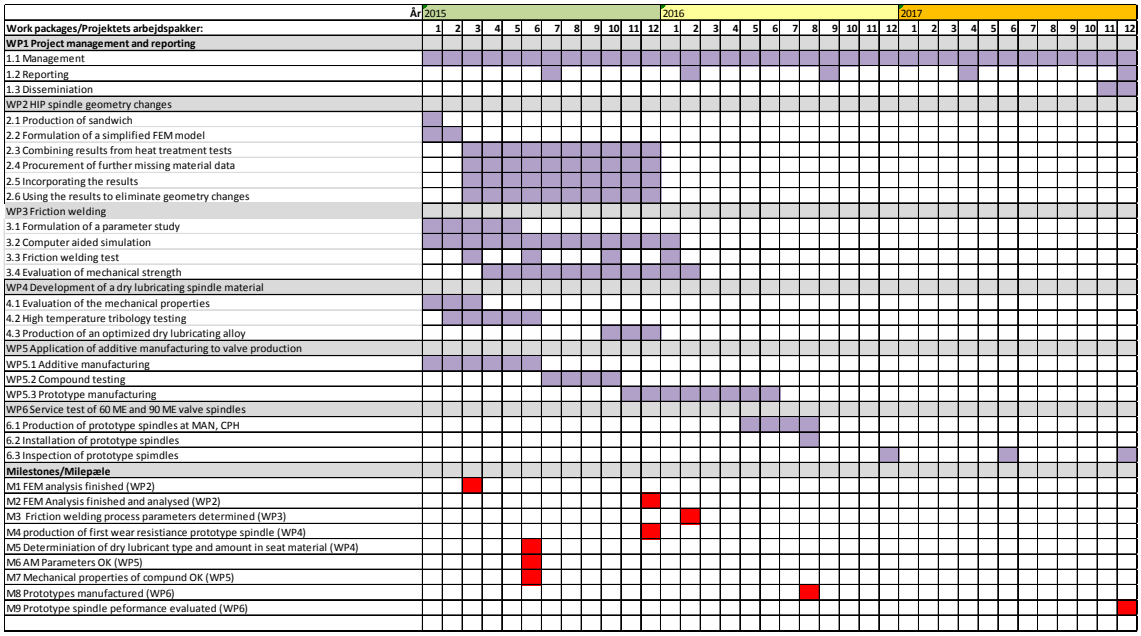

Figure 2 Initial project Gantt chart

In WP2 the objective is to analyse earlier service experience with compound spindles and based on Finite Element (FEM) simulations to develop a new design of the compound disc. The main task was to analyse and identify the root cause for a continuously developing plastic deformation of the disc experienced during former service tests. The deformation is unacceptable and prevents the compound spindle from becoming a commercial product. Only after determining the creep properties of the buffer and anticorrosion layers and using different numerical models the problem could be understood. The combination of materials with different thermal expansion, high creep rates of the HIP powder material, especially the Ni49Cr1Nb anti corrosion layer and cyclic thermal loading, were identified as the root cause. Alternative candidate buffer layer alloys were nominated to reduce the stress originating from differences in thermal expansion. However mechanical testing revealed a considerable reduction of the mechanical properties in the bonding zone at the base material. WP2 experienced considerable delays caused by the inability to simulate the high creep rates of the materials involved. Furthermore, after analysing models and results it was evident that the problem could not be solved without resource consuming creep testing of the involved materials. Finally it proved to be extremely difficult to quickly develop a new buffer layer compatible with the requirements set by the process parameters and neighbour materials. Consequently the related milestones M2 could not be met causing a serious set-back for the project. However, at the end of the project it was possible to stabilize the numerical model using the acquired material data. Hence, it was possible to outline a couple of paths to solve the underlying deformation problem. WP2 was performed by MDT with assistance from both DTU and SPS.

In WP3 the objective is by means of a Design of Experiment (DOE) test to identify the optimum friction welding parameters for a 60ME valve spindle stem and to transform the results to the larger 90ME spindle size. Further a numerical model for investigating the friction welding process had to be developed for joining the spindle head and stem, and a verification of the model had to be undertaken. This study was undertaken in collaboration between DTU and MDT and with Fricweld AB as a sub-supplier.
Satisfactory friction welding process parameters for the assembly of the spindle disc and stem were identified, and a simulation tool for the friction welding process was developed. The process parameters for two spindle sizes were identified and verified by both tensile- and fatigue testing. In both cases the mechanical properties of the welding zone were similar or superior to the base material properties. The friction welding simulation tool was developed successfully and verified by an instrumented welding test. The related milestone M3 was met within the set timeframe.

In WP4 the objective is to develop a spindle seat material including dry lubricating additives to counteract possible adhesive wear in case of operation on pure fuels. The approach to this objective was to blend the existing seat material powder with varying amounts of high temperature P/M dry lubricating candidate materials, and compact these with the HIP process. Ni-coated WS_2 and hBN powder in volume fractions of 3, 5 and 10% were applied, and tensile testing as well as metallurgical investigations were carried out on the compacted material. The mechanical properties in all cases were impaired to an unacceptable level and the microstructure revealed unexpected interaction between the dry lubricant and the seat material. Several attempts to procure WS_2 and hBN with an improved Ni-coating in order to counteract the interaction with the seat material failed. Also useful alternatives could not be identified. As a consequence further activities in WP4 were cancelled and the related milestone could not be met. WP4 was performed by SPS with assistance from MDT.

For WP5 the main goals were to develop printing parameters for -250µm powders, establish sintering parameters as well as test and verify mechanical properties of compound materials manufactured using the process. This manufacturing process development was then to be used for manufacturing a set of exhaust valve spindle prototypes.
Printing parameters were successfully developed to print the coarse powder with good and reliable results. However the sintering caused issues with chemistry of the sintered material that could not be overcome within the scope of this project. Instead the manufacturing of the prototypes would have to be done using an established and tested method that does not involve 3d-printing. The knowledge learned from this will be used to continue developing the printing and sintering process for other Ni-base alloys. This work will be continued by SPS after the project has ended. The results have been disseminated at project meetings.

As there were no final design set by MAN of the valve no prototype could be manufactured within the project.

As a consequence of the delays in the above WP's the activities in WP6 did not commence, and Milestone M6 – M9 were not met.

5. Project results and dissemination of results

5.1 WP2 HIP spindle geometry changes

The objective of this work package is to develop numerical models to analyse, understand and find a remedy for the permanent deformation observed during a previous HIP compound service test. The service tests have shown that the deformation continues to develop over time (Figure 3). The continuous development indicates that the problem cannot be solved by mechanical or thermal treatment of the produced component.

The problem is analysed by studying several simplifications of the HIP compound spindle. A simple model has several advantages over a complex model, e.g. isolate a single effect, simplified modelling, shorter simulation times, etc.

Work package 2 has been divided into six sub packages. Each sub package is reported separately.

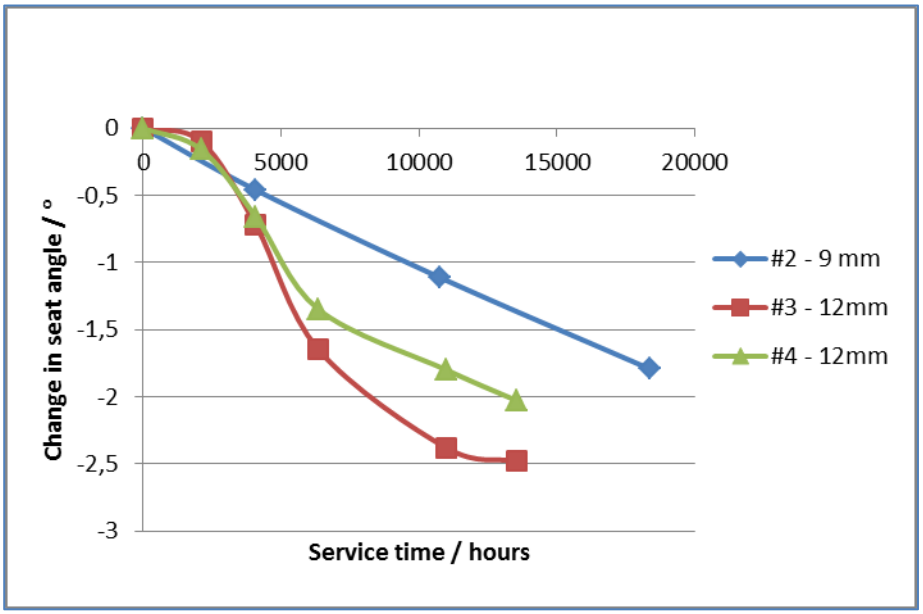

Figure 3 Measured seat angle development in service

5.1.1 WP2.1 Production of sandwich

Test specimens in the form of sandwich bars are produced to understand the permanent deformation occurring during heat treatment and in service. The specimens are cut from a produced prototype spindle (Figure 4). The specimens are then subjected to thermal loads by placing them in an oven with constant temperature over a period of two and a half month. At regular intervals some of the pieces were taken out and the length of the three material layers was measured with a Vernier calliper. The length of base material (SNCrW) was measured at the top the bar, the buffer (316L) layer was measured in the middle of the layer and the anti corrosion layer (Ni49Cr1Nb) at the bottom of the bar. The three layers are marked in Figure 5 with red, blue and green colour, respectively.

The high temperature furnace was preheated to 700°C which corresponds to the highest temperature the spindle experiences in service. The specimens were grouped in pairs and followed a sequence of control, to gain knowledge about the development of the deformation, see Table 1. The first group is taken out and measured approximately every fourth week. The first measurement was made after 10 days to capture any initial deformation. The results are shown in Figure 5. There is a degree of spread in the data, however a few conclusions can be drawn. The largest variation in results is found for the 316L material layer. Furthermore, specimen 1 and 3 differ from each whereas the specimen pairs that are checked fewer times confirm each other.

Table 1 Measurement schedule for sandwich test specimens

Specimen	Duration [Hours]			
1 & 3	262	650	1315.8	1842.3
2 & 4	x	650	x	1389.5
5 & 6	x	x	x	1845.5

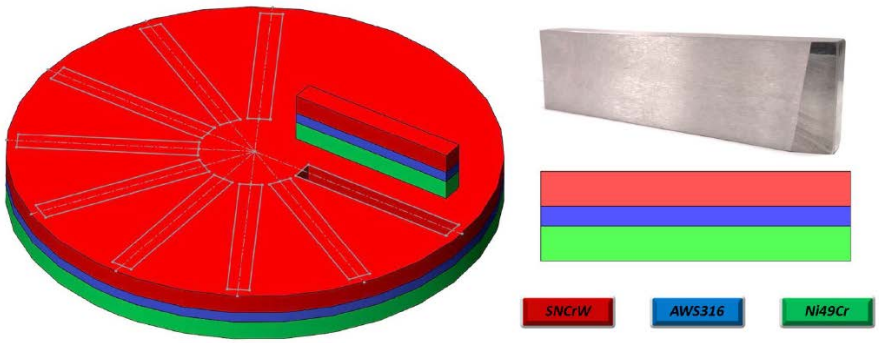

Figure 4 Production of test specimens from spindle prototype.

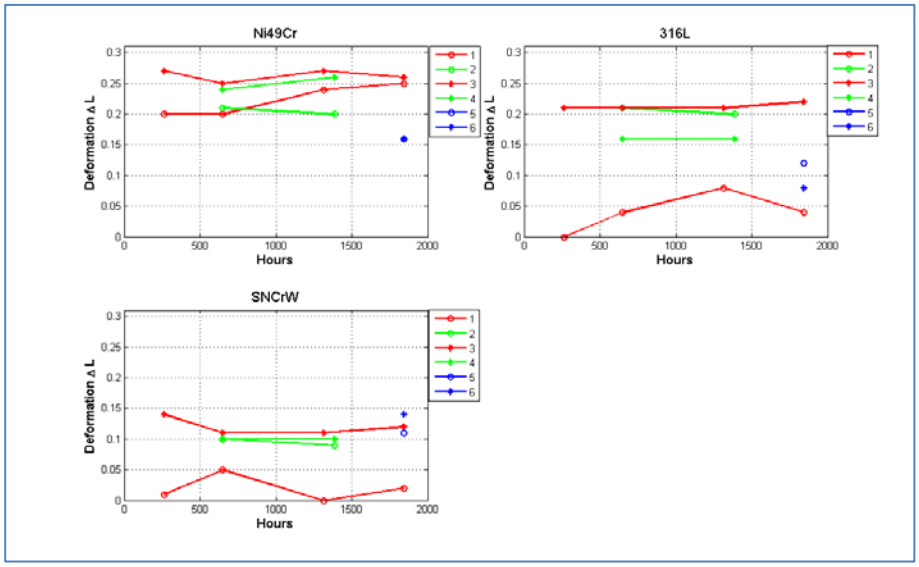

Figure 5 Results from oven test of sandwich specimens.

5.1.2 WP2.2 and WP2.3 Formulation of a simplified FEM model and Combining results from heat treatment tests

One major advantage of the sandwich specimen is that it is very simple geometry to model and very simple thermal loading, i.e. uniform heat load. The bar is constrained in the lengthwise direction at the left end and held at the lower left corner.

The model is subjected to one "full" load history corresponding to the real specimens; cool down from HIP, ramping up to service temperature followed by a 10 days in-service tempering stage and finally cooling down to room temperature again. The simulated deformations are then compared to the ones obtained from by the oven test. The results are seen in Table 2. Evidently, the simulated displacements are not consistent with what is seen in measurements.

Due to the simplicity of the modelled system it was concluded that the differences are down to insufficient knowledge about the material data. Both cyclic material properties and creep data [1].

Table 2 Displacement of the FE-model compared to measurements.

Material	Simulated	Measured
SNCrW	-0.0059	0.21
316L	-0.0003	0.1363
Ni49Cr	0.0024	0.0975

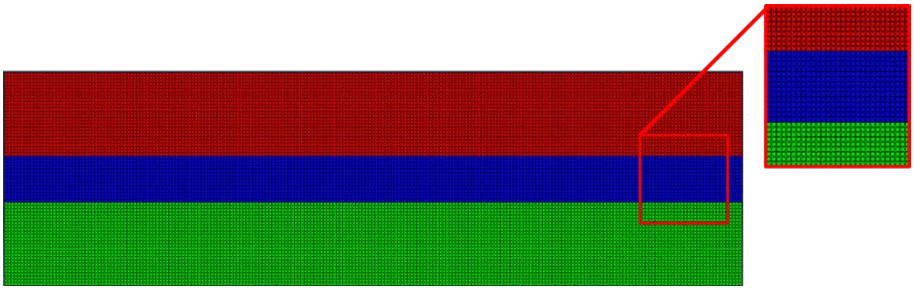

Figure 6 Numerical model of sandwich test specimen.

5.1.3 WP2.4 Procurement of further missing material data

Based on the initial numerical studies and previous attempts to build numerical models of the spindle, it was decide to obtain a complete set of material data, covering tensile testing, cyclic material characterisation and creep testing at elevated temperature. The test specimens was manufactured by project member SPS. Cyclic material characterisation was carried out project member DTU. Project member MDT's facilities for tensile testing at room temperature was used when appropriate.

Material characterization at elevated temperature

Two types of test geometries were designed for material characterisation at DTU. The compression tests were made on small cylinder with diameter ø7 mm and height 9 mm. The material characterisation was done using test pieces as shown in Figure 7. Powder material specimens were HIPed by SPS and machined by MDT.

Figure 8 shows the results from the second compression test series using the Gleeble test rig at DTU. The results from the first test series was checked against available sources and then disqualified. This provoked a re-calibration of the machine and the results second series are considered valid.

Material characterisation was interrupted by a rebuild of the test facilities at DTU. The rebuild has been delayed and it has not been possible to continue the testing within the time frame of the project.

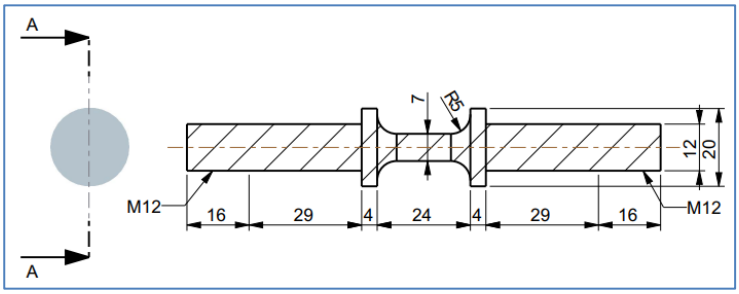

Figure 7 Defined specimen geometry for Gleeble testing.

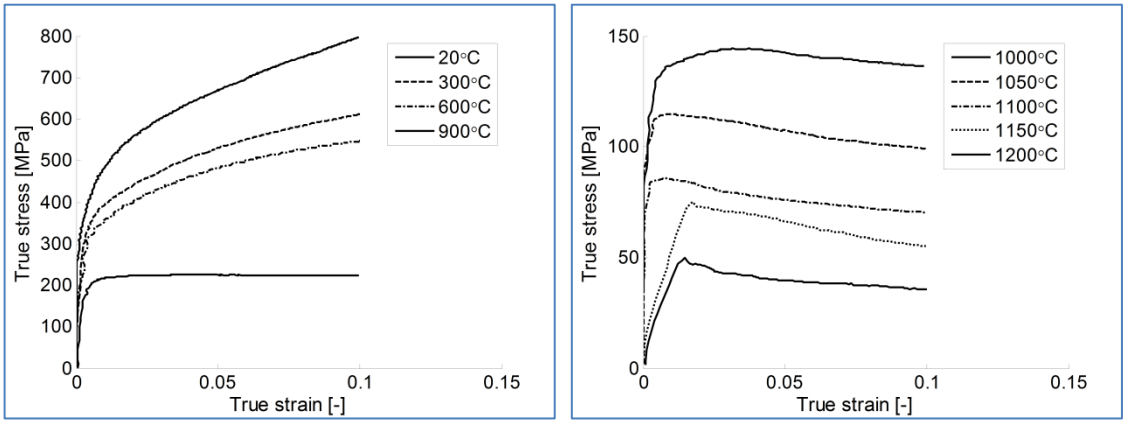

Figure 8 Results from Gleeble compression test of SNCrW.

Creep testing

Creep testing at high temperature is very expensive since it has to be done in a furnace and can take a long time. To produce results within the time frame of the project it was decided to use a simplified test procedure where three specimens were connected in series and loaded with a spring. The specimens were measured at one month intervals during the four month test period. The aim is to get a decent statistical base in relatively short time frame. The tests were made at a sub supplier SMT who had available capacity with furnaces set to 600, 650 and 700°C. This temperature range matches the operating conditions of the spindle.

The involved parties agreed on the test matrix shown in Table 3, where prioritised measure points are indicated with bold font. Temperature and load levels were chosen to match the conditions in the spindle. Time and cost considerations forced the test program to be further reduced to only include the powder materials 316L and Ni49Cr1Nb [2]. The test specimens are shown in Figure 9. The diameter varies depending on the yield stress of the material, since the test rig has a maximum capacity of 5500 N. Consequently, the 316L specimens are manufactured with a diameter of 5 mm and the Ni49Cr1Nb specimens have diameter of ø4 mm.

At the highest the temperature (700°C) the creep speeds are very high for the powder materials. For 316L only the specimens at 50% load survived to the first measurement. For Ni49Cr1Nb all tests failed before the first measurement. This means the primary and tertiary creep stages will have a relatively large influence on the estimate on the creep rate estimate, cf. Figure 10. Furthermore, the error originating from the one day resolution also has a larger influence in the beginning of the measurements. At 650°C all 316L specimens survive to the first measurement. Furthermore, all tests except the highest loaded (90% off yield) triple completed the entire test period. For Ni49Cr1Nb the situation at 650°C is the same as for 700°C, i.e. no tests triplets survived to the first measurement. At 600°C all 316L specimens survived to the end of the test. For Ni49Cr1Nb only the least loaded triplet (25% of yield) survived the test, the higher loaded tests failed before the first measurements.

The measured creep rate for 316L is shown in Figure 11. The data indicate that a power law creep law can be used to capture the measured creep behaviour, i.e. a linear relation in the log-log diagram,

$$\dot{\varepsilon}^{cr} = A\sigma^{n} \qquad \text{(EQ1)}$$

where $\dot{\varepsilon}^{cr}$ is the equivalent creep rate, σ is the equivalent stress and A and n are material constants. Figure 11 also includes a power law fit to the measured data. The material constants are listed at in Table 4.

The measured creep rate for Ni49Cr1Nb is shown in Figure 12. The measurements at 600°C and 650°C indicate a power law relation. However, the measured creep rates at 700°C fall on an almost horizontal line. The power law fit gives an exponent of 0,6 (Table 4). It can be concluded that the stress level in the Ni49Cr1Nb is too high to render reliable creep results. However, the results for 25% load at 600°C are considered valid and illustrate the level of creep for HIPed NI49Cr1Nb.

Table 3 Original test matrix for creep testing.

Material	Temperatur	Yield stress	Stress level in % of yield stress				
	[°C]	[MPa]	90 %	75 %	50 %	25 %	15 %
SNCrW	600	275	248	**206**	**138**	**69**	41
	650	253	227	**189**	**126**	**63**	38
	700	230	207	**173**	**115**	**58**	35
316	600	155	**140**	**116**	**78**	39	23
	650	145	**131**	**109**	**73**	36	22
	700	135	**122**	**101**	**68**	34	20
Ni49Cr1Nb	600	452	407	**339**	**226**	**113**	68
	650	402	362	**302**	**201**	**101**	60
	700	353	318	**265**	**176**	**88**	53
Ni40Cr35Nb	600	960	864	**720**	**480**	**240**	144
	650	880	792	**660**	**440**	**220**	132
	700	800	720	600	400	200	120

Table 4 Creep parameters obtained in measurements

Material	T	A	n
316L	600	7.5564E-23	6.3995
	650	5.7865E-20	5.6076
	700	8.6447E-17	4.5751
Ni49Cr1Nb	600	1.5764E-15	3.1874
	650	4.0288E-12	2.1986
	700	2.7589E-08	0.61792

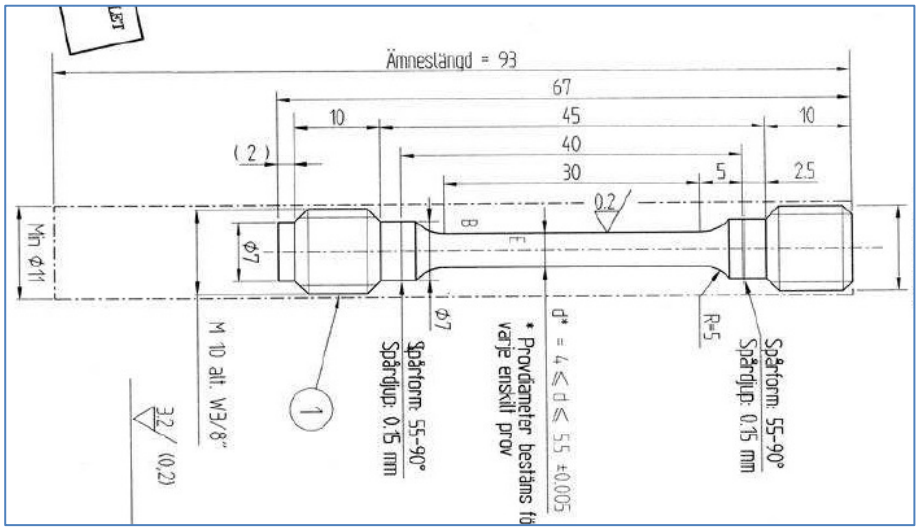

Figure 9 Test specimen geometry for creep testing.

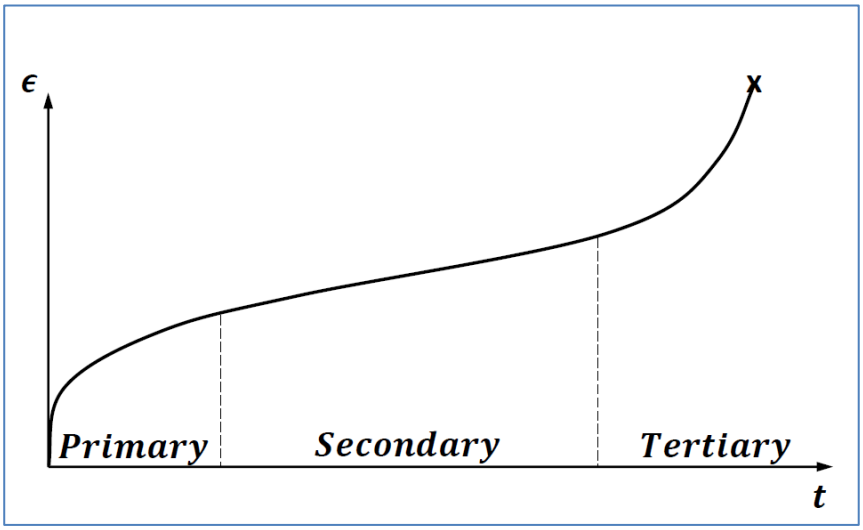

Figure 10 Creep stages.

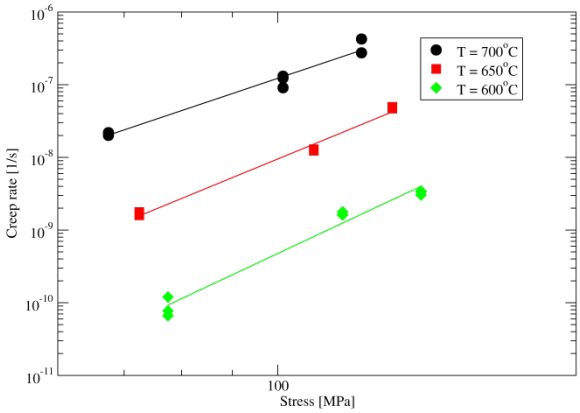

Figure 11 Measured 316L creep rate.

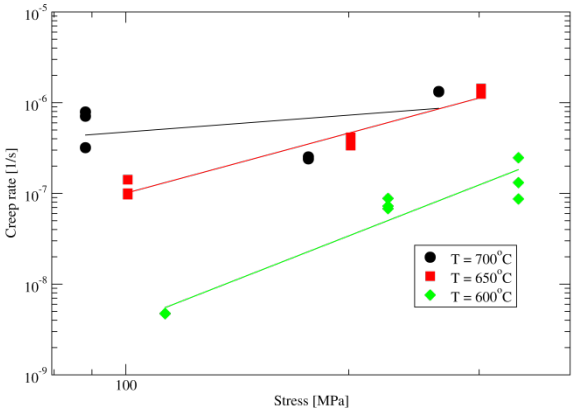

Figure 12 Measured Ni49Cr1Nb creep rate.

5.1.4 WP2.5 Incorporating the results

Comparison of material models

The measured creep parameters are compared to literature data for welded 316L in Figure 13. The creep parameters for welded 316L are listed in Table 5 [3]. It is evident that welded 316L has a stronger dependency on stress compared to HIP material.

For Ni49Cr1Nb no literature data has been found. However, the HIP material is held up against creep data for Nimonic81 which is considered a comparable alloy from a strength point of view. Creep data for Nimonic81 is listed in Table 5 and shown in Figure 14. The two materials are graphically compared in Figure 15. It is clear that HIPed powder Ni49Cr1Nb has a much higher creep rate compared to Nimonic81. The materials are in fact not comparable concerning creep. The results also indicate that the creep rate is higher for powder materials than welded materials, see Figure 16 where the creep rates, for the different materials at 600°C, are compared. The high creep rates leads to a very problematic numerical situation. The long simulation times in combination with high deformation rates require that mesh sizes, unit system and tolerances are properly set to achieve convergence in the numerical model. This has proven to be a very time consuming process.

Table 5 Creep parameters from literature [3].

Material	T	A	n
Welded 316L	600	$9.64 \cdot 10^{-32}$	10.28
	650	$3{,}83 \cdot 10^{-29}$	9,95
	700	$8.14 \cdot 10^{-26}$	9,05
Nimonic81	600	$3.21 \cdot 10^{-34}$	10.04
	700	$4.30 \cdot 10^{-19}$	4.95
	800	$3.84 \cdot 10^{-12}$	2.51

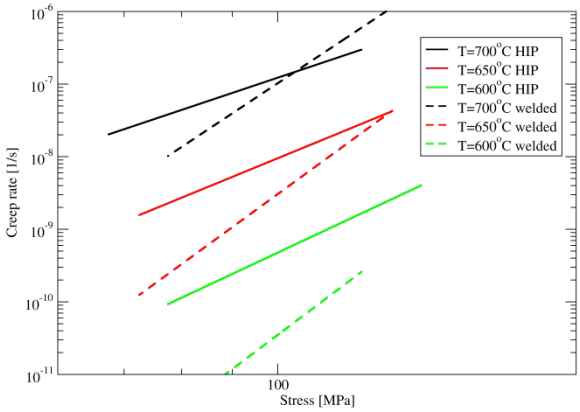

Figure 13 Measured creep rate for HIPed and welded [3] 316L.

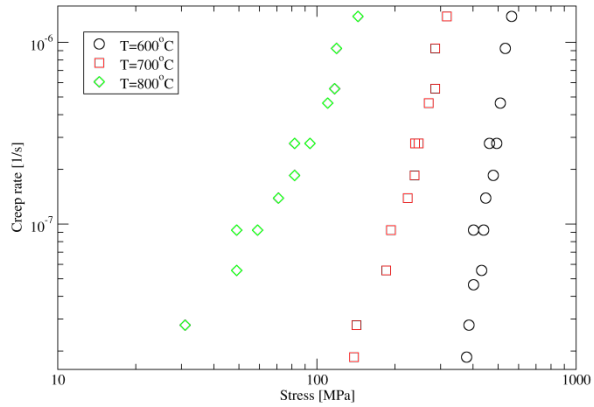

Figure 14 Measured creep rate for Nimonic81.

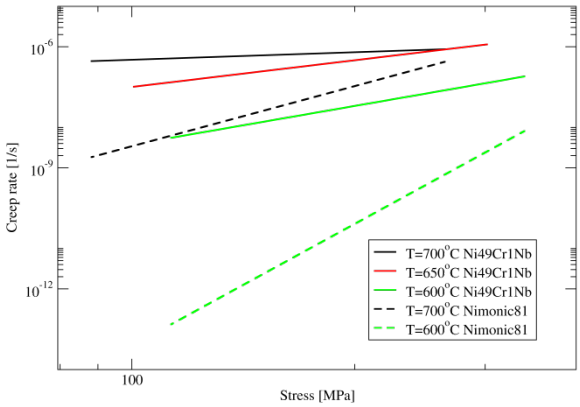

Figure 15 Measured creep rate for Ni49Cr1Nb vs Nimonic81.

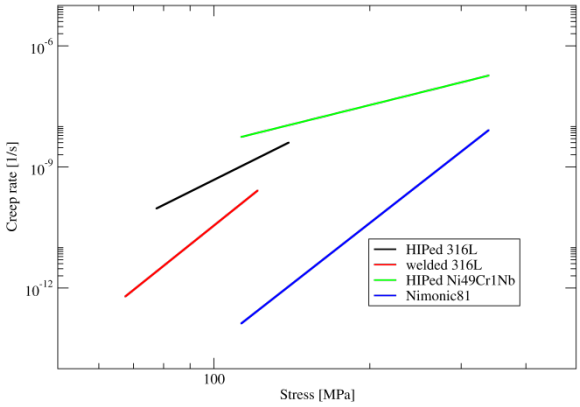

Figure 16 Creep rates at 600°C.

Simplified model with uniform thermal field

To investigate the root cause of the observed inelastic deformation a simplified FE model is developed, see Figure 17 [4]. The influence of the seat material is neglected. The model consists of ~260000 three node axisymmetric linear elements with 130000 nodes. The model is analysed using the Abaqus explicit solver. The three material layers are connected at the nodes, i.e. the layers share nodes. The model is held by constraining the nodes on the in the axial direction and the nodes on the centreline in the radial direction. The in-service mechanisms have been simplified so that the model experiences only a constant temperature field during the combustion, i.e. the entire spindle disc is uniformly heated up to 700°C, without external or internal forces applied.

The FE analysis covers the HIP stage and up to five cycles of normal operation. The HIP stage involves uniform cool down from 1100°C to 20°C. Each operating cycle describes heating up to 700°C, over 27 min, followed by a 260 h operating stage where the temperature is held constant at 700°C and finally a 30 min cooling down to 20°C stage. This means that the total simulation time covers 1305 h.

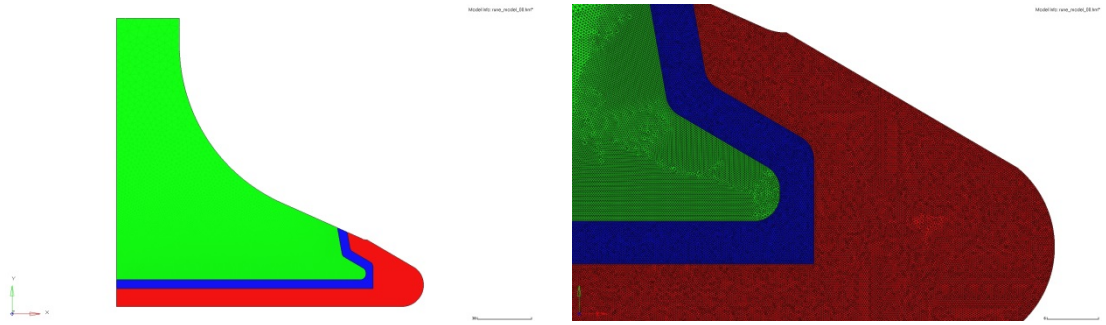

Figure 17 FE-model with uniform thermal load [4]

A power law creep model is applied to all three material layers. Due to excessive creep it has only been possible to obtain a converged solution using creep parameters from literature (Table 5).

Figure 18 shows how the seat angle develops through the simulation. The driving force behind the deformation is the difference in thermal expansion coefficient for the three materials (Figure 19). The base and buffer layer materials expand when spindle heats up. This induces tensile stress in the strong anti-corrosion layer. During operation the stresses in the Ni49Cr1Nb layer relaxes due to creep (Figure 20). The situation reverses as the spindle cools down, however, creep will not relax stresses at low temperature. The observed deformation is thus a consequence of stretching the strong Ni49Cr1Nb layer through creep.

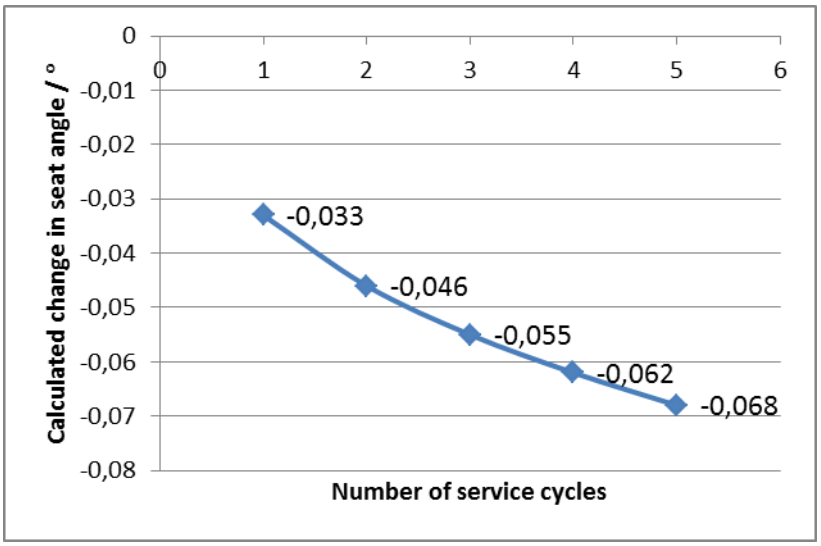

Figure 18 Cumulative calculated change in seat angle after each simulated service cycle.

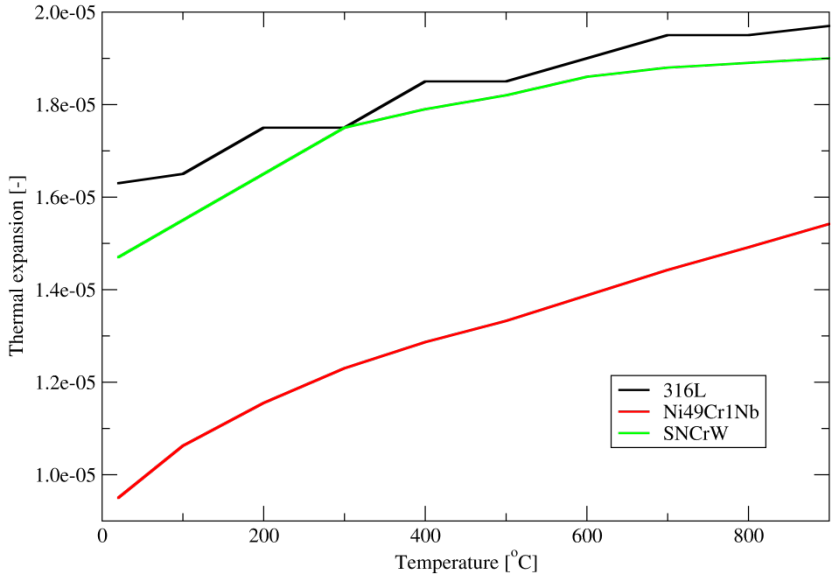

Figure 19 Thermal expansion coefficient for 316L, Ni49CrNb1 and SNCrW.

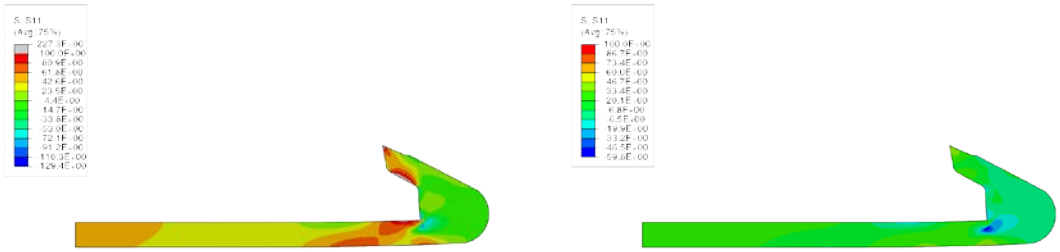

Figure 20 Radial stress during fifth operating cycle in the Ni49Cr1Nb layer after a) heating up and b) after operating.

Full model

The purpose of the full model is to include the influence of the thermal gradient. The applied thermal field during service is based on temperature measurements. The value of 700°C in the uniform field model is clearly an upper limit, see Figure 21.

The high creep rates found in the experiments and following numerical difficulties has restricted the use of creep data to measured data for 316L and only data for 600°C for Ni49Cr1Nb (Table 4). The simulation is run for 5 service cycles and the resulting deformation field is shown in Figure 22. The development of the seat angle is listed in and shown in Figure 23

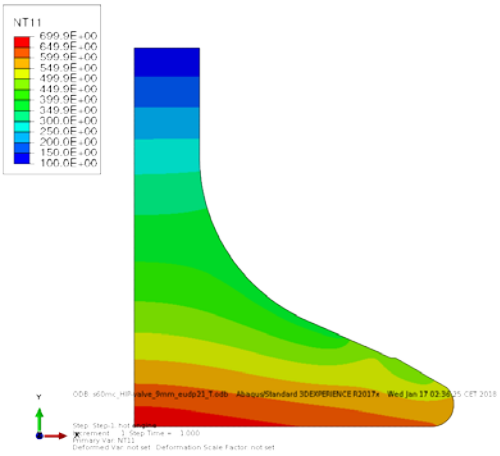

Figure 21 In service temperature field.

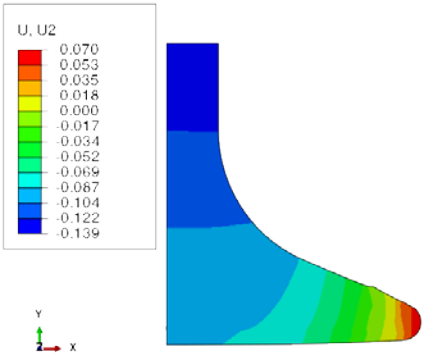

Figure 22 Axial deformation after 5 service cycles.

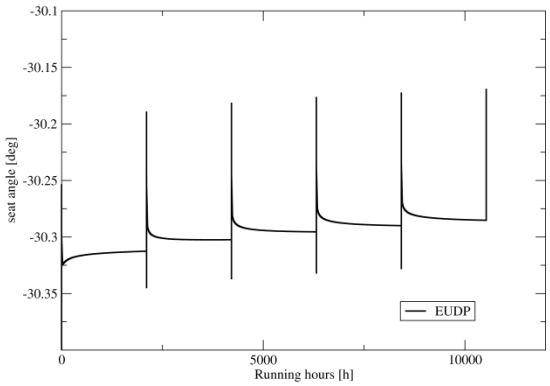

Figure 23 Seat angle development during service cycles.

5.1.5 WP2.6 Using the results to eliminate geometry changes

In the preceding section it was concluded that the driving force behind the deformation is the difference in thermal expansion between base (SNCrW), buffer (316L) and anti-corrosion (Ni49Cr1Nb) materials. There are several ways to reduce the influence of this difference. Some are briefly discussed in the following sub sections.

Changing material of buffer layer

By choosing a stronger buffer layer material with thermal expansion coefficient between SNCrW and Ni49Cr1Nb it should be possible to reduce the tensile stress driving the creep of the anti-corrosion layer. HIPed 654SMO was regarded as a promising candidate, see Figure 24. Initial material testing has been done within the project. Figure 25 shows results from tensile testing at room temperature. The strength of 654SMO exceeds the strength of 316L by far. N.b. tensile testing of compound specimens lead to fracture in the interface, cf sec. 5.4.2, which is unfavourable for application in the finished product.

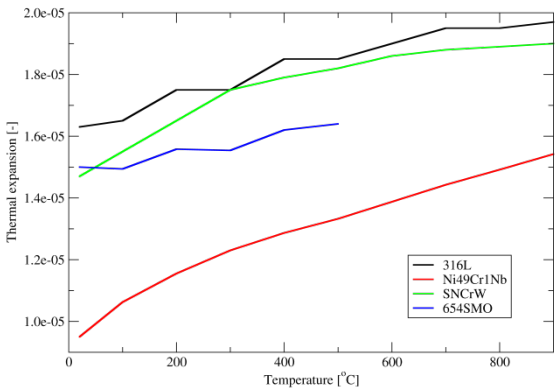

Figure 24 Thermal expansion coefficient for 654SMO.

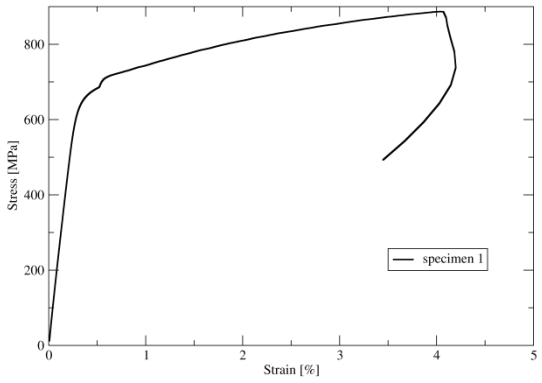

Figure 25 Tensile test of HIPed 654SMO.

Reduction of Ni49Cr1Nb volume.
Reducing the thickness of the Ni49Cr1Nb layer would lead to lower compressive stress in base material and buffer layer, thus reducing the deformation of the spindle. The effect can be seen comparing results from service tests with 9 and 12 mm Ni49Cr1Nb layers, cf. *Figure 3*.

Remove influence of difference in thermal expansion coefficient
The negative influence of the difference in thermal expansion coefficients can be removed my moving the buffer layer up to the colder shaft. On clear down side is that the use of Ni49Cr1Nb powder increases dramatically.

5.1.6 WP2 Dissemination of project results
The results from WP2 HIP spindle geometry changes have been disseminated at project meetings. Furthermore, results from simulations have presented at the 12th international conference on hot isostatic pressing in Sydney 2017 [4].

5.2 **WP3 Friction Welding**

5.2.1 WP3.1 Formulation of parameter study
Based on earlier attempts to friction weld exhaust valve spindles it was decided to apply pipe sections to be welded instead of full sections. Simulations of the stress level in service have confirmed that a section size with a bore of 50% of the outer diameter is showing a satisfactory safety margin.
For the optimization of the welding parameters we have taken a Design of Experiment (DOE) approach with three prominent process parameters each with two variables of each

- *Friction pressure*: pressure applied during rotation of the pipe.
- *Forge pressure*: pressure applied in the final step, after stopping the rotation.
- *Machine RPM*: rotations per minute (input: value set in the control panel / measured: real value)

In total the eight combinations of the above parameters were tested as well as and one supplementary test.
The evaluation of the DOE test is decided primarily to be based on the ductility level (elongation A5) obtained at mechanical testing of specimen across the welding zone. Secondarily the size and shape of the outside flash is applied as criteria in the evaluation.

5.2.2 WP3.2 Computer aided simulation
A thermomechanical model has been developed consisting of a heat transfer analysis for analyzing the temperatures within the parts during welding, and a quasi-static stress analysis for evaluating the final residual stresses and mechanical properties in the thermo-mechanically affected zone (TMAZ) of the welded part. The model is verified by comparison

with experiments performed at FRICWELD in Sweden (as explained in detail in this report). For the evolution of temperatures, the model has been verified by transient temperature measurements, where thermocouples were attached to the stationary part during the direct-drive friction welding process, see Figure 266a. The results from the simulations showed to be in very good agreement with the experiments, see Figure 266b.

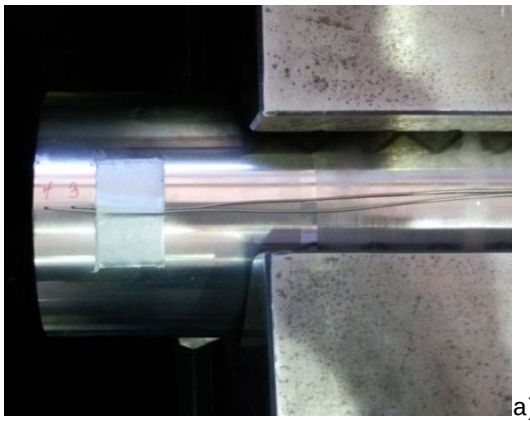
a)

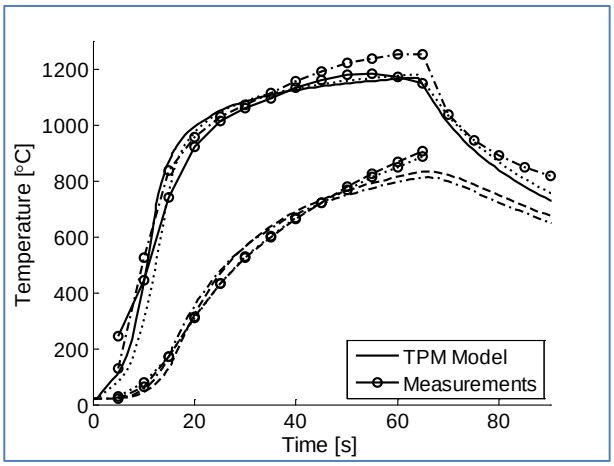

b)

Figure 26: a) Installation of the stationary part with the thermocouples 3 and 4 (1 and 2 on the back side). b) Comparison of the simulated and measured temperature evolution at the four points of the thermocouples (-1),(--2),(-.3),(..4) for the thermal model.

The mechanical model has been developed to predict the upsetting length and flash formation during the process. As shown in Figure 27: The resulting flash formation during the direct-drive friction welding obtained a) experimentally, b) numerically.

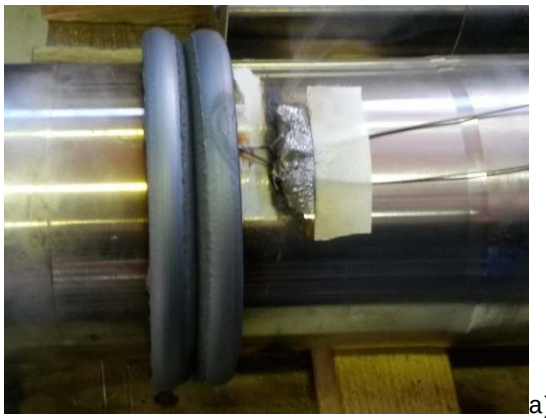
a)

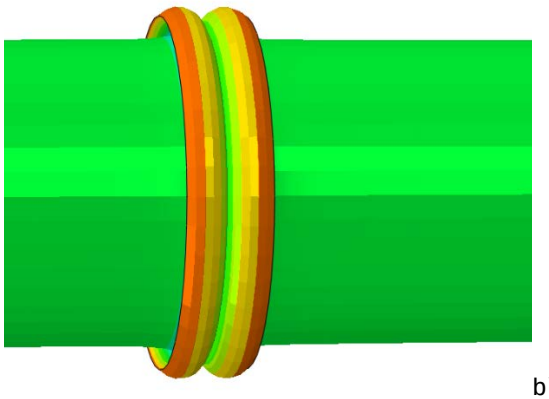
b)

Figure 27: The resulting flash formation during the direct-drive friction welding obtained a) experimentally, b) numerically.

Furthermore, a microstructural model has been implemented, which is able to predict the dynamic recrystallization during the friction welding process, see Figure 28. Images of the cuts were obtained by MDT within this work packages.

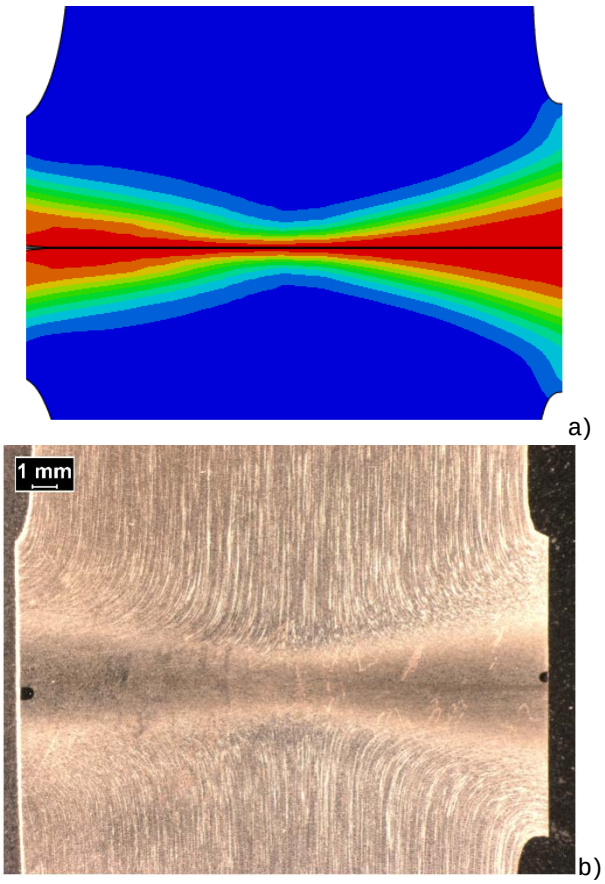

Figure 28: Comparison of the microstructure a) Obtained from the simulation (cut-out of Figure 27b), b) Picture from a cut-out of the friction welded part indicating the zone where recrystallization has occurred.

In addition to the development of the numerical model, material testing has been performed on the materials: HIP 316L, HIP Ni49Cr and SNCrW. The tests were performed on a thermo-mechanical simulator (Gleeble) and has supplied the project with temperature dependent stress – strain curves for the different materials used in the valve spindle.

The results within task 3.2 Computer aided simulation have been disseminated through a scientific publication [5] and a conference talk [6].

5.2.3 WP3.3 Friction welding test

The welding test was decided to be carried out for the spindle sizes 60MC/ME and 90MC/ME, starting with the smaller size with an expectation that the optimized parameters from the initial test could be transferred to the larger size. The welding would be carried out with identical materials on both sides being a forged austenitic valve steel designated SNCrW. The welded sections are Ø76/36mm and Ø112/54mm for the 60-bore and 90-bore size respectively.

As sub-supplier the company FRICWELD AB, Hällefors, Sweden was chosen. The friction welding machine applied for the test is a 200T “direct drive” system from ETA Technology Pvt. Ltd. (Bangalore, India). The W.O. No of the machine is WF01170734 (year 2012-2013). During each test all relevant process parameters are logged in the system computer and the process progress made visible on the computer screen (Figure 299).

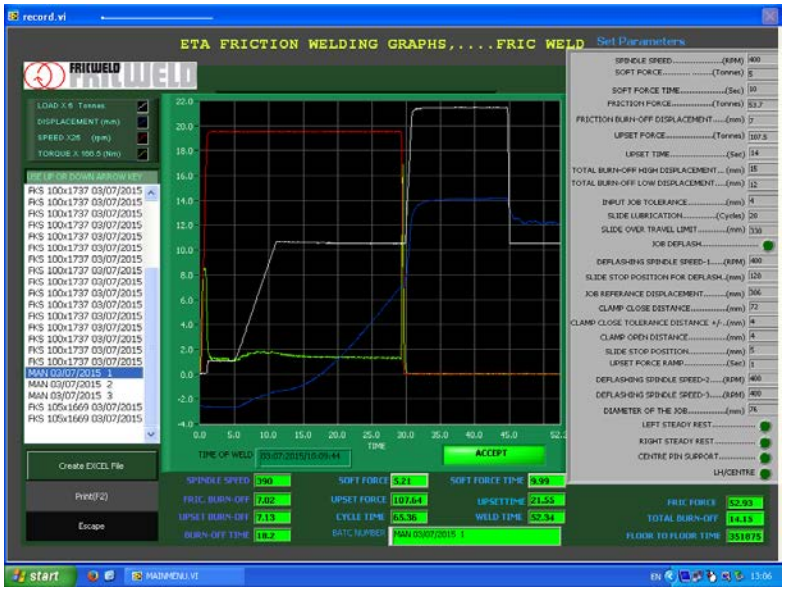

Figure 29: Screen of weld control unit with on-line data of main process parameters.

Subsequent to some initial test to verify suitable levels for the DOE process parameters the flw. set of parameter combinations were performed (Table 6).

Table 6: Combination of process parameters at the initial DOE test samples

Sample nr	Friction pressure [Mpa]	Forge pressure [MPa]	Machine RPM (in-put)	Machine RPM (mea-sured)	Upset length [mm]	Measured upset [mm]
1	125	240	350	350	3.5	9.2
2	150	180	300	300	8.5	10.6
3	150	300	300	300	2.0	7.3
4	100	180	400	375	8.7	14.7
5	150	180	400	375	4.3	6.4
6	150	300	400	375	7.0	13.7
7	100	300	300	300	3.0	13.7
8	100	300	400	375	0.2	9.2
9	100	180	300	300	3.5	8.3

Each sample subsequently was inspected visually and the shape of the external welding zone was documented. After cutting out the welded zone to a suitable length for preparing samples for mechanical testing, the samples were sectioned axially into two halves for inspection of the inner and outer flash development.
In a next step metallurgical samples were extracted of the welding zone and 3 tensile test specimens (M16 x Ø10mm) with the welding zone positioned in the middle of the gauge length were machined from each of the above mentioned 9 samples. The 3 specimen were radially positioned at the inner, outer and intermediate part of the welding zone.
Since the valve spindle will be heat treated at 700°C for 4 hrs as one of the final production steps the tensile test specimen and some of the metallurgical specimen were heat treated according to the above condition.
The evaluation leading to the nomination of the optimum process parameters to be fatigue tested involved the criteria stated in a prioritized order.

1. Elongation value of the tensile test incl. visual inspection for possible surface cracks on the gauge length
2. Microstructural evaluation of the bonding zone (presence of oxides and molten sections)
3. Appearance of flash formation

Macroscopy and microscopy

The flash appearance and dimensions have been evaluated externally and on axial sections from the welding zone. The criteria for a satisfactory flash geometry is a fully developed convex flash as this condition assures a high certainty that oxides are removed from the bonding line.

Both the fully developed flash of sample 4 and 6 and a partly developed flash of sample 5 is shown in Figure 30Figure 30.

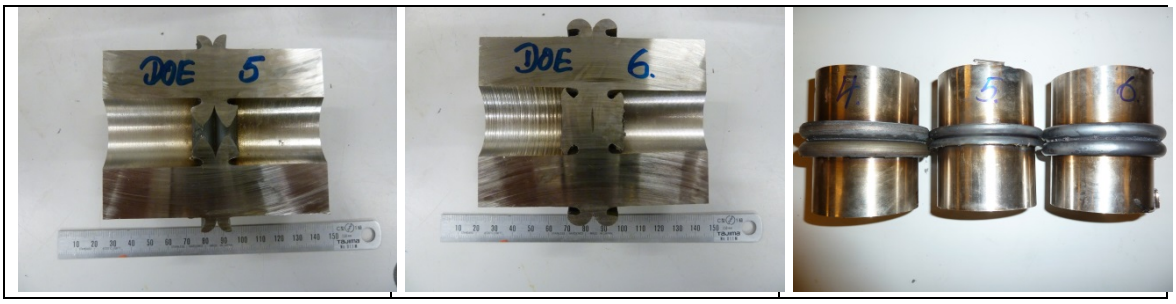

Figure 30: Welding flash geometry on a selection of samples

The investigation of the microstructure at the bonding zone primarily is aiming at identifying possible defects, e.g. missing bonding, metal oxides or indications of molten metal. In all cases the mechanical properties of the bonding zone will be deteriorated.

The microstructure adjacent to the bonding zone in all samples shows a significant amount of deformation and related recrystallization (Figure 31 & 32). The bonding zone was detectable and in case of sample 2 and 5 recrystallization of a possible molten area could be detected. Otherwise no significant defects could be identified.

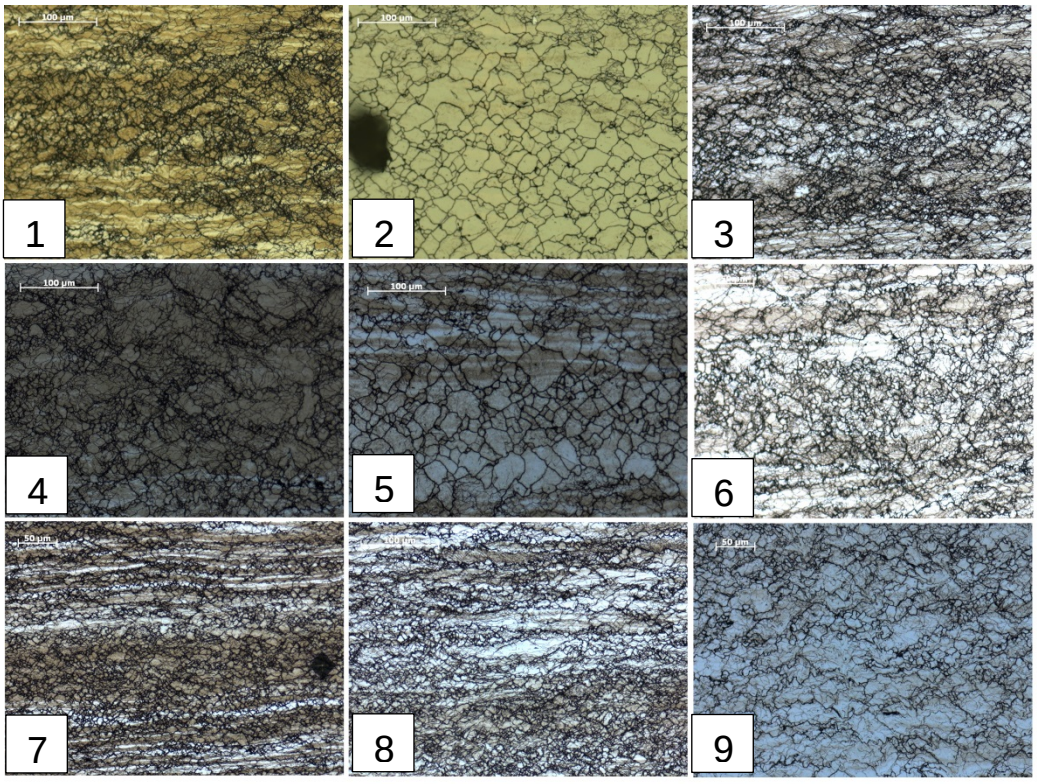

Figure 31 Microstructure at the bonding zone of all weld samples

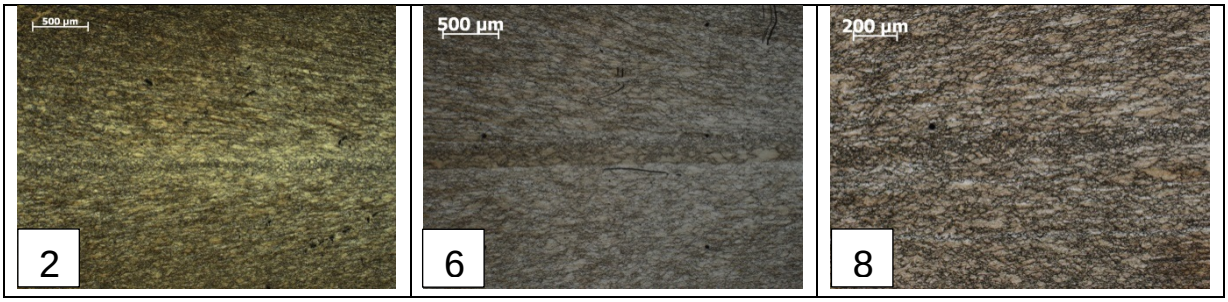

Figure 32: Microstructure at the bonding zone of the DOE samples

5.2.4 WP3.4 Evaluation of mechanical strength

Tensile testing of the standard M16 x Ø10mm specimen was carried out on an Instron 300kN tensile testing machine (5587) at room temperature. The mechanical properties showed no significant dependency on the radial position in the welding zone for which reason the average result from the 3 tests of each sample are shown in Table 7.

Table 7: Mechanical properties of welded and heat treated samples

Sample nr	**Rm (MPa)**	**Rp0.2 (MPa)**	**Elongation (%)**	**Z (%)**	**Tested specimen with surface cracks after tests**
1	765.0	427.0	34.5	41.4	0
2	761.0	420.3	34.0	39.2	0
3	765.3	428.3	33.6	40.6	0
4	760.3	418.3	34.6	40.8	0
5	755.7	426.3	37.5	45.8	0
6	771.7	433.3	35.6	41.3	0
7	769.7	436.3	35.6	42.0	1
8	764.0	433.7	39.8	46.5	0
9	761.7	416.7	36.2	38.2	3
Specification for SNCrW	>700	>350	>26	>45	N/A

The properties of the 9 samples appear to be rather identical with minor variations. In all cases the specified requirements are fulfilled and the fracture position is not related to the bonding zone. Minor cracks on the gauge length after testing were found on specimen from sample 7 and 9.

As expected the DOE review did not show any significant trend as to which combination of the process parameters are to be favored, however high friction pressure and high rotational speed have a beneficial effect on the elongation values.

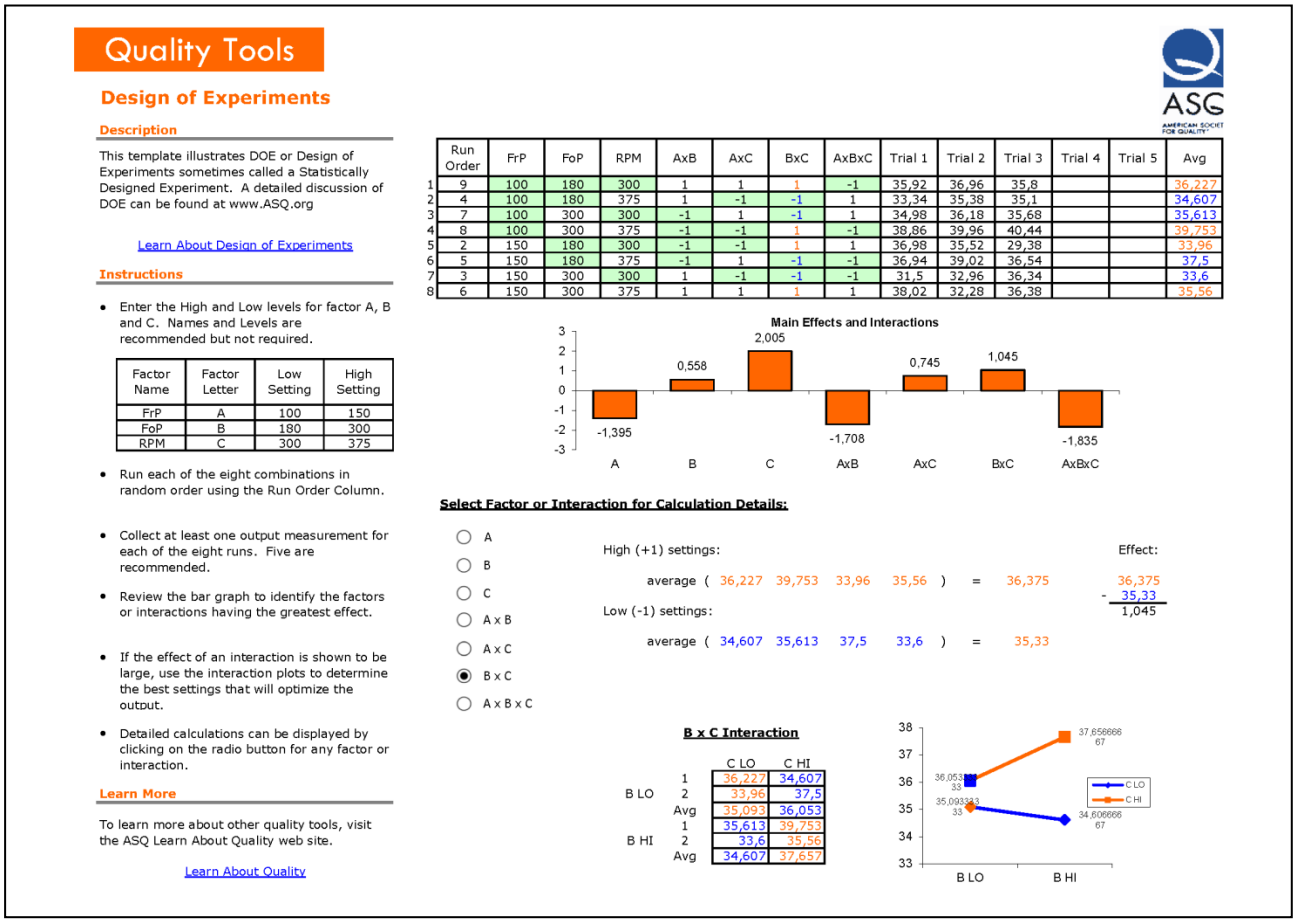

Figure 33: DOE evaluation sheet

In addition to the microstructural evaluation the metallurgical samples have been used to document the hardness profile in the welding zone.
In the as welded condition the influence of the welding on the hardness in the axial direction is very limited while we see no general trend for the hardness profile in the radial direction.
Both in the as welded and as welded & heat treated condition the variation in hardness in the radial direction is limited to 50 – 60 HV.

Selection of the optimum parameters

Taking the above results into account the following the route for selecting the sample having the optimum parameters is as follows.

- Sample 2 and 5 are excluded because of signs of recrystallization / melting in the welding zone
- Sample 7 and 9 are excluded for the presence of surface cracks on the tensile specimens
- From a DOE analysis of the elongation value as a function of friction pressure, forge pressure and
  Machine RPM measured (see Enclosure 6), it appears that high friction pressure and high machine RPM have a beneficial effect on the elongation values
- This therefore points to Sample 6 and 8, which are both produced with high forge pressure (300 MPa) and high measured machine RPM (375)

Based on the development of the flash the process parameters of sample 6 were decided as the optimum.

Welding test 90ME

Due to the capacity limit of 100t during friction heating and 200t during upsetting it was not possible to apply similar process parameters as sample 6.

Working at maximum load capacities only minor modifications of the upset length showed the required flash development leading to the below process parameter.

Table 8: Welding parameters of 90ME size

Sample nr	Friction pressure [Mpa]	Forge pressure [MPa]	Machine RPM (input)	Machine RPM (measured)	Upset length [mm]	Measured upset [mm]
2-90ME	130	260	400	390	6	13,2

A 160mm long section of sample 2 with the welding position at the center was prepared for taking out 18 specimens for tensile and fatigue testing, as well as for an investigation of the microstructure. All specimens were heat treated at 700^{o}C for 4 hrs. Out of these 3 pcs were applied for tensile testing. The tensile test results showed minor variations and below are shown the average properties which large and by are according to the specification of the base material.

Table 9: Mechanical properties of heat treated sample 2-90ME

Sample nr	Rm (MPa)	Rp0.2 (MPa)	Elongation (%)	Z (%)	surface cracks after tests
2-90ME	761	425	25,3	44,3	0
Specifications for SNCrW	>700	>350	>26	>45	N/A

Inspection of the microstructure in the welding zone did not reveal any significant defects.

Fatigue testing

The simulation of the stresses in the spindle stem is indicating a mean stress close to 0 MPa, during actual service for which reason is was decided to carry out fatigue testing with R=-1. Testing is carried out with standard Ø16 x Ø10 x 160mm test specimen on a 100kN Instron fatigue testing machine (8801) at room temperature by the staircase method.
For reference testing was carried out on specimen from monolithic base material, while 20 specimen were tested with specimen extracted at the outer periphery of the 60ME samples welded with the process parameters of sample no. 6, while 7 pcs were tested from the outer periphery and 8 pcs tested from the inner periphery of sample 2-90ME. All specimens were heat treated at 700^{o}C for 4 hrs.
Below are presented the results of both the reference test as well as the results of the friction welding samples.

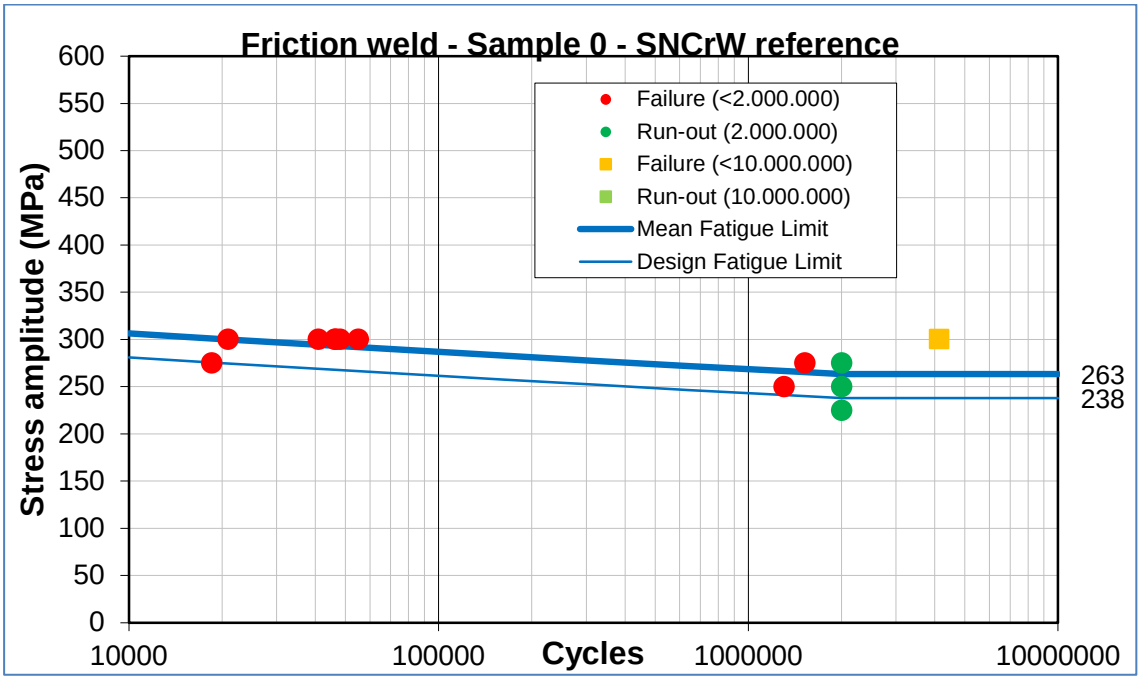

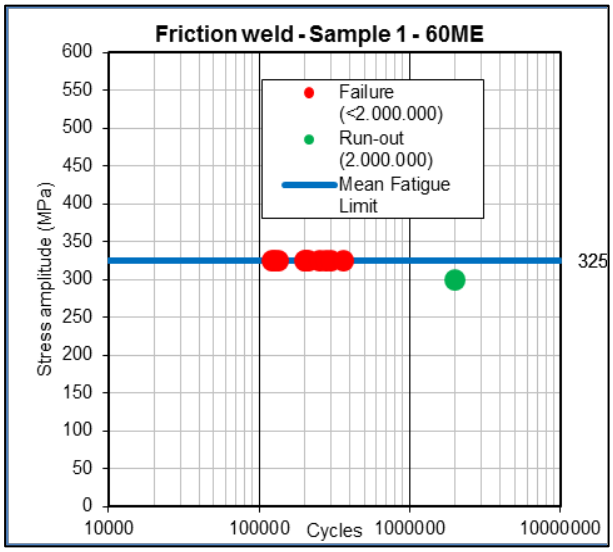

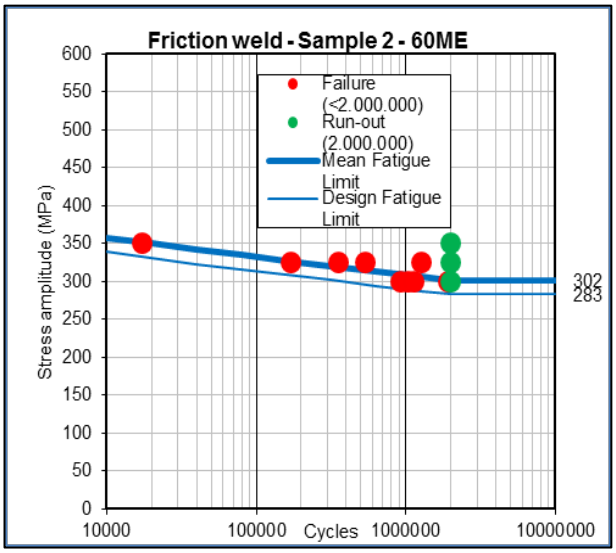

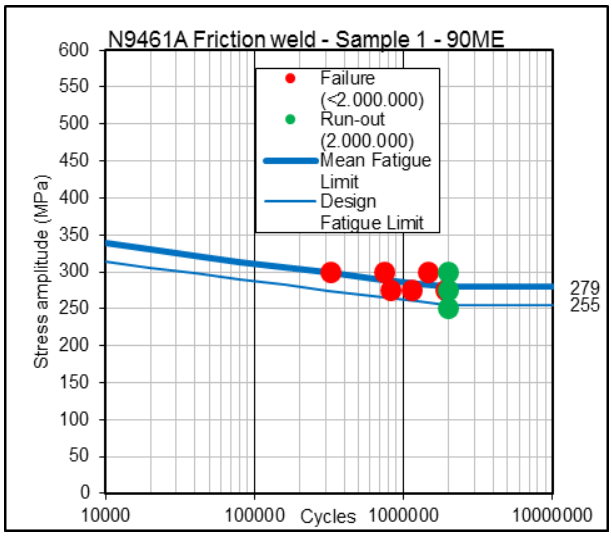

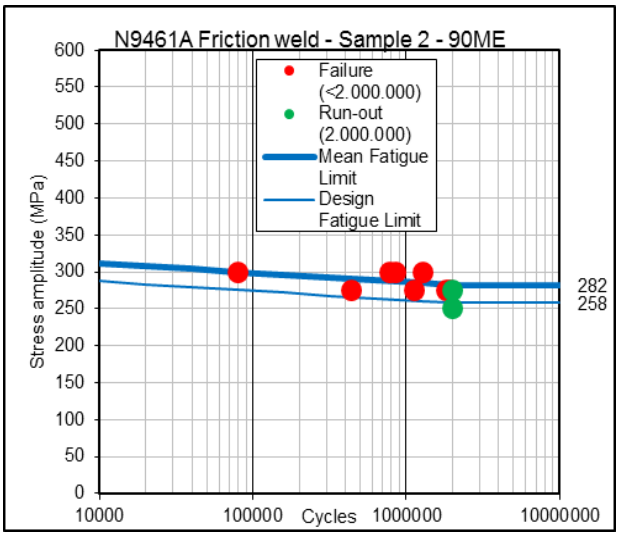

Figure 34: Fatigue test results - SNCrW reference and Sample 1 & 2 from sizes 60 & 90ME

The results indicate a design fatigue limit of 238 MPa While the friction welded samples show a design fatigue limit of 283 MPa and 255 MPa for the sizes 60ME and 90ME respectively.

All fractures during fatigue testing are positioned outside the bonding zone for which reason the applied welding parameters are fully approved.

5.3 WP4 Development of a dry lubricating spindle material

The plan for the WP was to start with manufacturing and testing several different material candidates in three low volume mixtures with the spindle seat material. Once suitable material candidates that showed promise with regards to mechanical properties were identified these would then be evaluated using high temperature tribological testing. When a material concept was found that met the mechanical properties and showed good performance in tribological testing an optimized version would be manufactured and verified. This optimized alloy would then be used in manufacturing of the valve spindle prototypes.

5.3.1 WP 4.1 Evaluation of the mechanical properties

This part of the WP was early delayed due to problems in sourcing Ni-coated hBN and Ni-coated WS_2 powders for manufacturing of new test materials. The initial test included mixtures of 3, 5 and 10 vol.% with the Ni40Cr3.5Nb seat alloy HIP'ed at 1100°C/3 hrs. The mean particle size being 50 µm of the lubricant and <250 µm of the seat alloy. Each of the mixtures microstructures subsequently was investigated under the light optical microscope (LOM) and scanning electron microscope (SEM), see Figure 34 and 35.

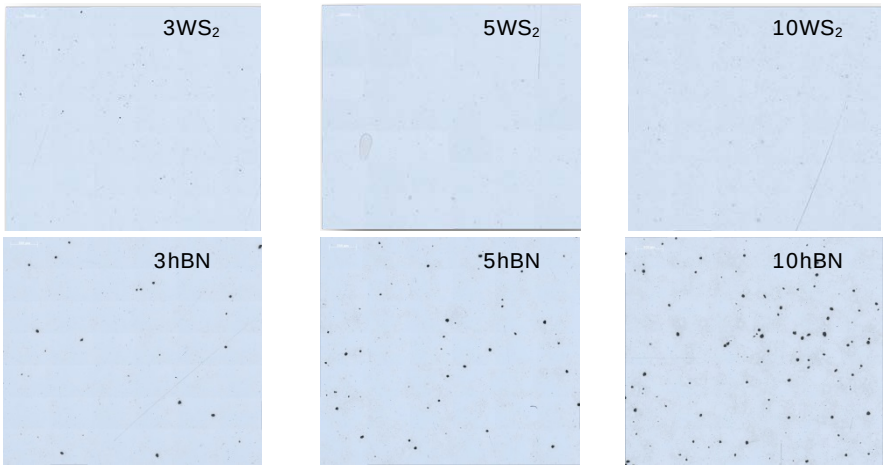

Figure 35: LOM of mixtures with WS_2 and hBN

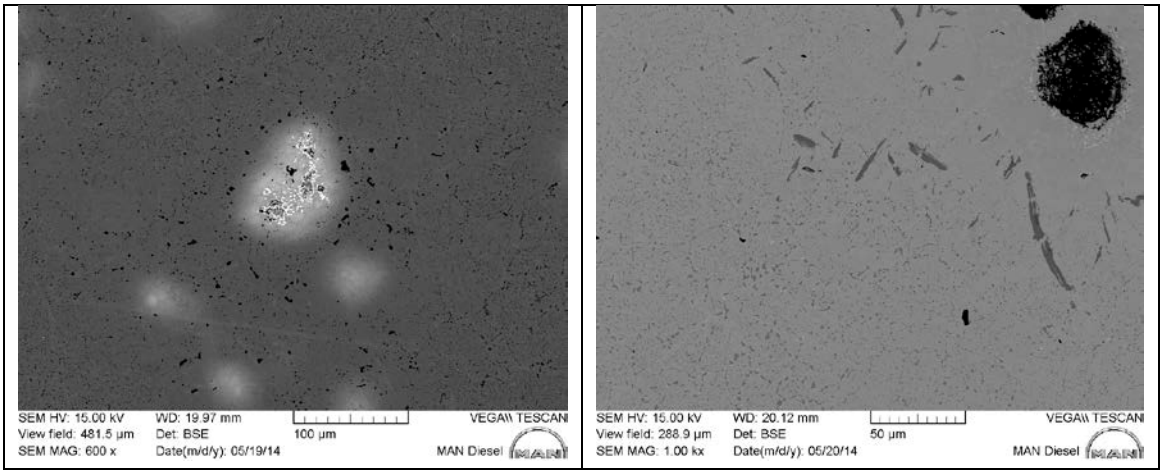

Figure 36: SEM of embedded WS_2 (left)and hBN (right) particles

Further hardness testing was carried out on the as-HIP material. Finally all samples were heat treated at 700 °C/4 hrs corresponding to the age hardening of the seat material and tensile testing was carried out subsequently, the results are presented in Figure 36 & 37.

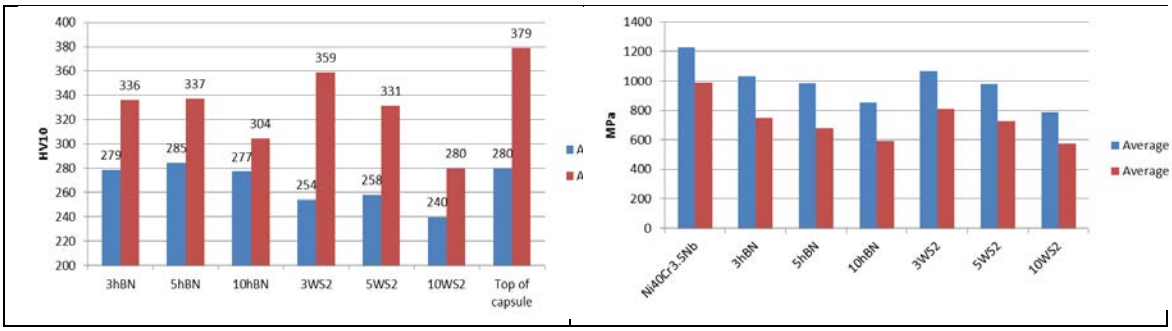

Figure 37: Sample hardness (left) and UTS and YS of aged samples (right)

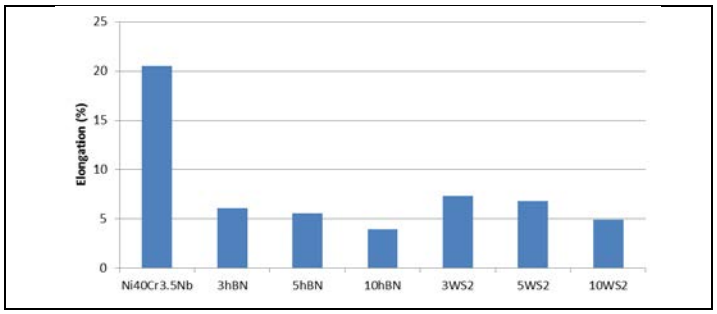

Figure 38: Tensile elongation of aged samples

From the investigation of the microstructure it was evident that both the WS_2 and the hBN have shown an interaction with the base material despite the Ni coating. Since WS_2 is decomposing at temperatures above approximately 800 ^{o}C it can be expected that diffusion of the Ni-coating has exposed WS_2 to the base material, initiating it decomposition which is evident in Figure 36, in case of hBN the Ni coating did not prevent interaction with the base material, as CrB phases are detected adjacent to the hBN particles which however as expected have shown to be stable during the HIP process.

As illustrated in above Figure 37 and Figure 38 the mechanical properties are affected significantly by adding the dry lubricant. It has been expected that the properties were impaired to some degree, however the remarkable reduction of the tensile elongation at all levels were not expected and are considered unacceptable for the present application.

Most likely the cause for this degradation is the partly decomposition and interaction with the base material.

As a subsequent step it was decided to identify a producer of Ni-coated hBN with a documented quality of the Ni-coating. Despite a large number of attempts especially on the US market it showed to be impossible to find the required quality and as a next step the decision was taken to move forward with an uncoated hBN powder instead, at least that would eliminate the problematic Ni-coating. This caused an initial 6-month delay of the WP but due to the a original time plan for the WP with plenty of room it would only delay the end of WP4 by 2 months and not affect the total time of the project.

The initial tensile testing of the samples showed however additional deterioration of especially the tensile elongation, see Table 10.

Due to the very poor mechanical properties the microstructure of the material has not been evaluated. It is believed that the uncoated hBN contaminated the surface of the powder particles of the Ni-alloy during mixing of the powders. During HIP the hBN effectively then hinders any bonding between the powder particles and the ductility of the material is greatly reduced.

Table 10: Mechanical properties of HIPed Ni40Cr3,5Nb + hBN composite material

		YS [MPa]	UTS [MPa]	A [%]
Ni-coated hBN	3%	751	1035	6
	5%	682	984	5,5
	10%	596	858	3,9
Non-coated hBN	3%	609	877	3
	5%	712	819	1
	10%	-	430	0

It can be concluded that un-coated hBN cannot be used for the manufacturing of the self-lubricating MMC materials.
Eventually it turned out that sourcing of suitable powders was more difficult that first believed. A number of potential suppliers for various suitable candidate materials were contacted without any success. Other suppliers of Ni-coated hBN was found but they all used a electroless coating process which results in the poor properties found in previous project. The decision was taken to cancel the WP due to issues with properties of current material as well as finding a source and supplier for alternate materials without possible environmental issues as e.g. various fluorides and BaCr2O4.

5.3.2 WP 4.2 High temperature tribology testing
Cancelled, see WP 4.1

5.3.3 WP 4.3 Production of an optimized dry lubricating alloy
Cancelled, see WP 4.1

5.4 **WP5 Application of additive manufacturing to valve production**

In WP5 the basic printing and pre sintering parameters for Ni40Cr3.5NB and Ni49Cr1Nb materials would be developed for the application in the HIP compound disc assembly (Figure 39). Printing and pre-sintering parameters were to be established that resulted in good dimension accuracy and material chemistry. Once this is done, monolithic pre-sintered and HIPed material samples and compound samples where to be manufactured and mechanical properties would be verified using tensile testing. The basic parameters from this WP would then be used for the manufacturing of the valve spindle prototypes.

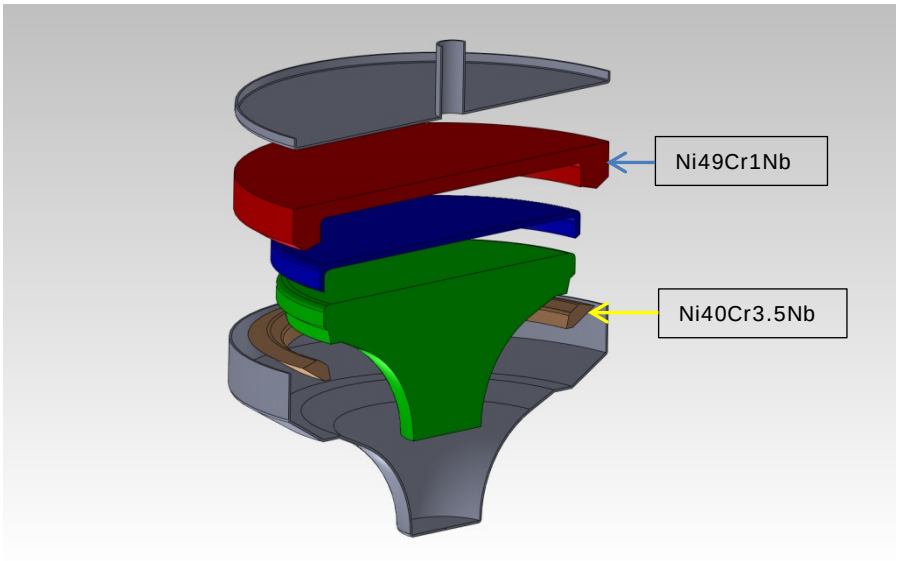

Figure 39 Assembly of the HIP compound spindle disc

5.4.1 WP5.1 Additive manufacturing

During period one the basic build parameters in the 3d-printing was performed successfully. The printing was performed using an ExOne M-flex binder jet printer. To keep the total manufacturing costs of the valve spindle as low as possible powder yield is very important. Normally these machines use a powder <40µm in particle size and the average powder particle size manufactured is normally well above that. This means a significant amount of powder, possibly more than 50% would need to be sieved away and not be used in manufacturing. Furthermore, a finer powder could cause issues with mechanical properties of the material due to the large surface area picking up excessive amounts of oxygen, a well-known problem in powder metallurgical HIP.

To eliminate the aforementioned issues a significant test program of printing parameters was performed. A test geometry designed for this project was used to verify building parameters. The process used powder bed binder jetting technique, and for this to work properly the thickness and integrity of each powder layer in combination with binder content and the rate it is applied must be adapted to the powder used. CAD drawings and printed samples of the test geometry can be seen in Figure 40.

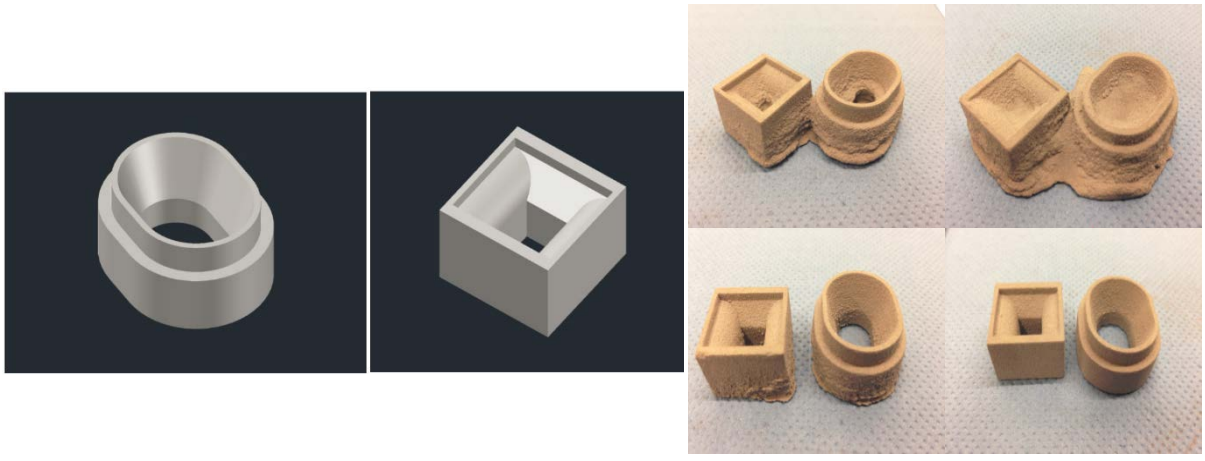

Figure 40: CAD models of test pieces and examples of printed samples .

To verify that the geometries that will be used in production can be printed and pre-sintered with sufficient quality sever

Al test rings with a similar geometry as will be used in the spindles have been built and pre-sintered successfully, see Figure 41. The tests verified that the developed printing parameters together with a basic pre-sintering can manufacture bodies of sufficient quality.

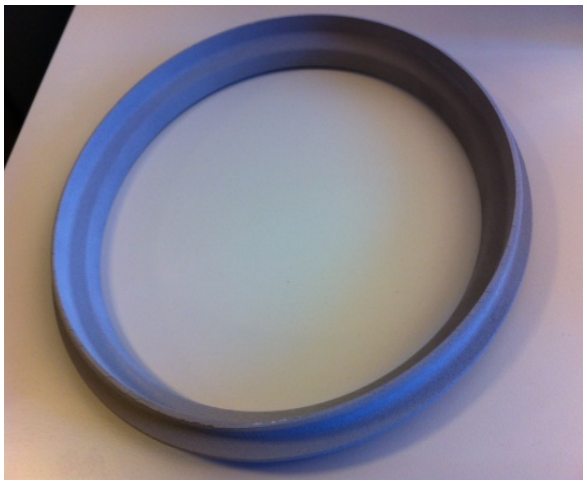

Figure 41: Printed and sintered Ni40Cr3.5Nb material for use in the seat area of the valve spindle.

The established printing parameters work for all the powders that will potentially be printed during manufacturing, Ni49Cr1Nb. Ni40Cr3.5Nb and 316L. Sintering of the test pieces for material and compound material testing and characterization went according to plan.
The pre-sintering of the printed parts work well with none or very minor distortion/shrinkage of the printed parts. However, issues arose regarding the chemistry of the pre- sintered material.
During sintering it was initially expected that any oxygen pick up during printing and curing the water based binder wouldn't be an issue as it would be reduced during the sintering in hydrogen. Also, it was assumed that any carbon from the binder would be easily removed during de-binding process in conjunction with sintering. This had been tested and verified before on other Ni-base alloys e.g. 625. However, for the two Ni-base alloys and the Fe-base alloy used in this project the initial results showed a significant increase in oxygen and carbon content of the pre-sintered material compared to the powder used.
It was initially anticipated that the issues were caused by improper atmosphere control during sintering, mainly too high dew point i.e. too high oxygen content in the furnace. A lot of effort was put in to make sure the atmosphere was as good as possible. New sintering trays were acquired, a new drying process of the furnace was implemented, improved gas control are just a few of the initiatives implemented to counteract the issues. The following sintering cycle yielded little or no improvement despite the improved atmosphere in the furnace. See Table 11 for a comparison of powder chemistry to as-sintered material.

Table 11: C, N and O-content of powder and pre-sintered samples compared to specification.

		C [%]		N [%]		O [ppm]	
316L	**Powder spec**	**0,012**		**0,05**		**100**	
316L	1st batch Ø7mm	0,14	↗	0,003	↘	38	↘
316L	Max acc. Spec	0,03				200	
Ni49Cr1Nb	**Powder spec**	**0,005**		**0,028**		**199**	
Ni49Cr1Nb	1st batch Ø23,5	0,043	↗	0,03	=	348	↗
Ni49Cr1Nb	Max acc. MAN spec.	0,02	↗	0,05		200	
Ni40Cr3.5Nb	**Powder spec**	**0,004**		**0,019**		**125**	
Ni40Cr3.5Nb	1st batch Ø23,5	0,047	↗	0,027	↗	759	↗
Ni40Cr3.5Nb	Max acc. MAN spec.	0,02		0,05		200	

As can be seen the levels of C and O are too high while N is not. The levels of C and O will have an adverse effect on the ductility and toughness of the material. It was concluded that the atmosphere in the furnace was not the cause of the poor chemistry and that a sintering study needs to be performed to solve the issue. An optimized de-binding and sintering cycle had to be developed.

The third period most of the work ended up being focused on solving the issue with C and O-content. As mentioned earlier in previous R&D work on Ni-base alloys performed, this has not been an issue but since the maximum amount of carbon allowed in the alloys used in this product is about 10 times lower it turned out to be an issue, especially in combination with the chemistry of the powders.

It has been established that the source of the oxygen is the water in the binder which oxidizes the surface of the powder particles during the curing process. The source of the carbon is the organic constitute in the binder that reacts with the Cr, Nb and Ti in the material to form stable carbides effectively binding the carbon.

A lot of work was performed with regards to printing parameters to reduce binder content which is the source of C and O increase. Furthermore, the sintering parameters were modified in order to be able to increase the oxygen and carbon removal by introducing an additional isotherm and longer holding time at the de-binding stage. The basis of this decision was done on thermogravimetric analysis (TGA) done on the binder used. From this analysis result it could be concluded at which temperatures the binder constituents start to vaporize. The analysis cannot be shared to confidentially restrictions from ExOne. In Table 12 some examples from the study are shown indicating that there were still issues with both the C and O-content. Results from different sample sizes are also shown.

Table 12: O, N and C content of powder and sintered materials pre-sintered in optimized sintering cycle.

		C [%]		N [%]		O [ppm]	
316L	**Powder spec**	**0,012**		**0,05**		**100**	
316L	2nd batch Ø7mm	0,045	↗	0,0015	↘	37	↘
316L	2nd batch Ø23,5	0,037	↗	<0,0005	↘	251	↗
Ni49Cr1Nb	**Powder spec**	**0,005**		**0,028**		**199**	
Ni49Cr1Nb	2nd batch Ø23,5	0,034	↗	0,027	=	349	↗
Ni49Cr1Nb	2nd batch flake	0,043	↗	0,018	=	282	↗

As can be seen the C-content in the 316L material was reduced somewhat but it's still too high. The O-content is still well controlled for the smaller sample size but much too high for the larger sample. Thermodynamic calculations have shown that the oxides formed in 316L can be reduced in the sintering cycle used. As can be seen though, the amount of oxygen being removed in 316L depends on the section size. A prolonged isotherm at sintering tem-

perature can solve the issue with the oxygen content, however the C-content will require additional measures.
As for the Ni-base alloys there are only minor improvements. The slightly lower C-content is most likely a result of an improved de-binding procedure. However, the O-content is still exceeding the maximum level. To further reduce carbon, the carbides formed during sintering will need to be dissolved, however they are thermodynamically stable at the sintering temperatures used.
Further tests to optimize the sintering cycle were performed. Small changes to the de-binding procedure and the temperature ramp were introduced in combination with higher sintering temperatures to aid oxide reduction. These changes had again a negligible effect on the chemistry of the sintered material. A potential solution to reduce the C-uptake was however found. By optimizing the printing parameters the amount of binder was reduced, hereby considerably lowering the carbon content to an extend which solved the issue with the high C-content in the sintered material. In Table 13 are shown the analysis of the as-printed and cured samples i.e. not sintered. As can be seen the C and O-content is drastically reduced. Unfortunately, the O-content is still too high to be able to produce a useful material.

Table 13: C, O and N content of as-cured material.

		C[%]		N[%]		O[ppm]	
Ni49Cr1Nb	Standard print	0,2		0,057		912	
Ni49Cr1Nb	Optimized print	0,12		0,054		629	

We have co-operated with the 3d-printing equipment manufacturer to solve the problem, and concluded that the standard binder cannot be applied. Instead we continue with new experimental binders under development by the printer manufacturer in an attempt hereby to solve the issues during sintering the 3D-printed parts.
Although the experimental binders that have shown promising results on other materials, it seems that even with this new binder we still cannot meet the desired maximum limits on C and O content.
As the previous investigations indicated that the C-content could be improved by applying a lower binder content during printing, tests were initiated using low binder (LB), medium binder (MB) and a high binder (HB) content. The binder content in LB-samples is slightly higher compared to the optimized print parameters from Table 13. The MB is the same as standard print from Table 13 and HB is slightly above. In Table 14 the results from tests made with the new binder are shown.

Table 14: C, N and O-content of pre-sintered materials.

		C [%]		N [%]		O [ppm]	
Ni49Cr1Nb	**Powder**	**0,005**		**0,028**		**199**	
Ni49Cr1Nb	2nd batch Ø23,5	0,034	↗	0,027	=	349	↗
Ni49Cr1Nb	New binder LB	0,021	↗	0,039	↗	339	↗
Ni49Cr1Nb	New binder MB	0,022	↗	0,038	↗	374	↗
Ni49Cr1Nb	New binder HB	0,033	↗	0,041	↗	336	↗
Ni40Cr3.5Nb	**Powder**	**0,005**		**0,028**		**125**	
Ni40Cr3.5Nb	2nd batch Ø23,5	0,034	↗	0,027	=	349	↗
Ni40Cr3.5Nb	New binder LB	0,018	↗	0,045	↗	212	↗
Ni40Cr3.5Nb	New binder MB	0,009	↗	0,053	↗	312	↗
Ni40Cr3.5Nb	New binder HB	0,014	↗	0,038	↗	207	↗

As can be seen there is an improvement on both C and O-content in the sintered samples. For the Ni40Cr3.5Nb -alloy all the samples had an approved C-content and for the Ni49Cr1Nb material there was a reduction in carbon content although not sufficient. If the new binder can produce green bodies of sufficient strength in combination with the optimized printing parameters this could solve the C-issue. There is still however the issue with the

oxygen content in both materials. The Ni40Cr3.5Nb material, which showed a low amount of oxygen in the powder is large and by exceeding the limit in two samples whereas the oxygen content is considerably the limit in the MB-version. In case of the Ni49Cr1Nb material the oxygen content is unchanged with the new binder.

From the all work done we currently, with Ni40Cr3.5Nb and Ni49Cr1Nb, see no way forward with the 3d-printing process. It is primarily the O-content that is the issue and despite trying to optimize the process, the affinity to oxygen in the material and the thermodynamic stability of the oxides at the relatively low sintering temperatures used here, is an obstacle which cannot be solved within the frames of this project. To solve this a considerable effort needs to invest on the binder, printing, curing, de-binding and sintering side. It was therefore decided that any prototypes manufactured in WP6 would have to be done with a proven technology developed before this project started, and that was used to manufacture the very first quad metal valve spindles

5.4.2 WP5.2 Compound testing

Despite the fact that there were issues in sintering of samples for compound testing there was also work done on finding an alternative to the 316L buffer layer between the valve steel and the Ni-base alloys. A brief test done on IN625 as buffer layer based on the rationale that the low solubility of C in Ni would give an effective barrier to C-diffusion in to the Ni49Cr1Nb and Ni40Cr3.5Nb materials. Based on the tensile test results of the compound samples it is evident that the alloy is not suitable due to the low ductility of the bond, see table x. The strength of the bond is satisfactory while the tensile elongation is unacceptable.

Table 15: Mechanical properties of tensile test on compound samples with 316l (reference) and IN625 as buffer layer.

	YS [Mpa]	**UTS [Mpa]**	**A [%]**	**Z [%]**
316L	332	675	29	72
	388	684	23	69
	370	678	29,5	72
IN625	352	563	5	3,5
	358	570	5	8
	359	553	5,5	4

The work with finding a replacement for 316L as buffer layer became even more important when early results from the modelling showed that the 316L buffer layer was a contributing factor for the smiling valve issue

The major part of the work during period 4 was on identifying and testing new alternatives for buffer layer. The work has consisted of sample manufacturing, testing and microstructural characterization of compound test pieces. The aim was to find an alloy that has a coefficient of thermal expansion between Ni49Cr1Nb and SNCrW, has a high strength as well as serving as a good diffusion barrier for carbon. A literature survey and study has been made to identify three possible candidates.

In a first series three new materials were tested: 654SMO, IN617b and a 100µm brush plated Ni-coating as buffer layer between SNCrW and Ni49Cr1Nb. Table 16 is showing the mechanical properties of the as-HIPed compound samples together with two reference tests of 316L. It is evident that the 316L materials results in a much higher ductility over the interface. The Ni-base alloy IN617b and the Ni-coating show similar performance as the IN625 material presented in Table 15.

Table 16: Mechanical properties of compound samples with alternative buffer layers.

	YS [Mpa]	UTS [Mpa]	A [%]	Z [%]
316L- ref.	363	679	27	71
316L - new	301	614	23	74
654SMO	463	701	8	41
IN617b	428	616	3	7
Ni-coating	430	607	3	5

Studying the microstructure if the samples it becomes clear as to why none of the samples comes close to 316L. Figure 42 shows micrographs from all the samples in the fracture zone and/or at the interface.

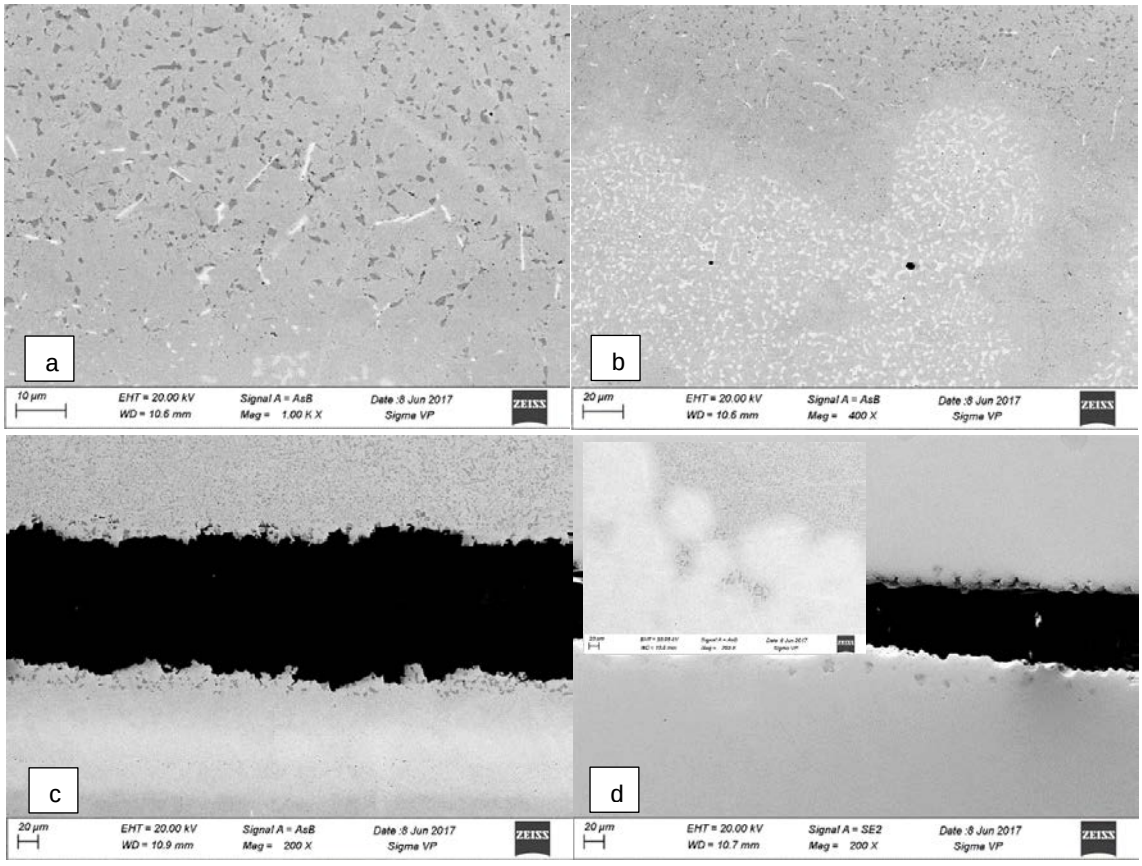

Figure 42: Micrographs of compound samples with buffer layer 654SMO (a & b), Ni-coating (c) and 617b (d).

The sample with 654SMO as interface fractured in the valve steel well away from the interface. The fracture occurred just outside the measurement length (L0), hence the low elongation value. Studying the microstructure at the two interfaces two main precipitates can be found, Cr-carbide (dark) and an intermetallic phase (bright) assumed to be sigma phase. The relatively low cooling rate during HIP has caused a high amount of sigma phase precipitation. The amount is higher closer to the Ni49Cr1Nb material. This is most likely a consequence of N-diffusion from 654SMO to the Ni49Cr1Nb material reducing the amount of N in 654SMO, thereby increasing the susceptibility of sigma phase formation. Moving towards the interface to SNCrW material the amount of sigma phase gets lower. Here instead there are carbides formed close to the interface to a level which is similar to what is formed in 316L to SNCrW interface investigated in previous project. At first glance the 654SMO can seem like a promising buffer material but unfortunately the susceptibility to sigma phase formation at ageing

during manufacturing and operating temperatures will lead even higher amounts of sigma phase and consequently drastically reduce toughness and ductility.
The fracture in the sample with Ni-coating as buffer layer has occurred in or near the Ni-Ni49Cr1Nb interface. Here there is a 30µm large zone with a large amount of Cr-rich carbides extending in to the Ni49Cr1Nb material. The fracture and occurred straight through the zone rich in Cr-carbides.
The fracture in the material with IN617b as buffer layer has occurred in or near the IN617b-SNCrW interface. At the interface, extending in to IN617b a <10µm reaction zone very rich in carbides has formed. The zone contains mostly Mo-rich carbides and some Cr-rich carbides. A likely reason for the high amount of carbides in a relatively narrow band along the interface is the low solubility of carbon in Ni. The C-activity in the Ni-base material becomes very high even when relatively small amount of C has diffused into the alloy. The activity/low solubility causes the reaction with Mo and Cr to form carbides. The mechanism is the same in IN625.
Besides experimental work on the new buffer layer the work in period 5 was mainly continued search for alternative materials, reporting and making sure we are ready for prototype manufacturing, it where to happen after this project is over.

5.4.3 WP5.3 Prototype manufacturing

Little to none of the work originally planned for WP5.3 could be performed i.e. manufacturing of the prototypes. This because no final design to solve the smiling valve issue of the valve could be established.

6. Utilization of project results

6.1 WP2 HIP spindle geometry changes

The developed model of the HIP compound spindle can, at the end of the project, be used to study different remedies for countering the continuously developing inelastic deformation. The combination of differences in thermal expansion between the involved materials, the unexpected high creep rates, especially for Ni49Cr1Nb, and the cyclic thermal loading has been identified as the root cause of the deformation. This conclusion limits the commercial applicability of the HIP compound concept in its present form.
It is concluded that creep properties of the involved materials are crucial when designing HIP components, consisting of two or more materials, to be used for high temperature applications. This knowledge will save resources for the project members in the future.

6.2 WP3 Friction welding

The project participants can utilize the developed thermomechanical model for friction welding processes applied in their future products, where the simulation tool can be used to uncover the process window of the actual combination of material and geometry before performing actual welding experiments. This is beneficial for the companies since money is saved on not performing expensive friction welding tests.
The application of a friction welded hollow stem furthermore is a prerequisite for the development of the active cooled exhaust valve spindle which presently is an objective in an internal MDT project.

6.3 WP4 Development of a dry lubricating spindle material, WP5 Application of additive manufacturing to valve production

Unfortunately for SPS the technology developed in this project will not be used commercially for manufacturing valve spindles. Much of the work performed was very specific to the alloys used in the valve and SPS do not use or foresee a use of them in any other products.
There might be a few learnings from the printing and sintering process development that SPS can apply on other materials and products.
The printing and sintering process used in this project was patent pending by Sandvik prior to this project.

7. Project conclusion and perspective

The overall project objective of developing a novel heavy duty valve spindle capable of handling high heat load and being service tested, has not been fulfilled.
Although considerable effort has been spent on being able to simulate the service performance of the HIP compound design this was only achieved at the end of the project due to unexpected challenges related to both the model and material properties.
Further the important development in the production processes to reduce cost only partly were solved as 3-D printing and pre-sintering of compound components could not fulfil the material specifications, while the friction welding process parameters of the spindle stem could be identified and successfully simulated.
Valuable results have been achieved with respect to modelling compound materials under creep conditions and useful basic knowledge is obtained in the field of 3-D printing coarse powder fractions with subsequent pre-sintering. Further friction welding of a hollow stem has been successfully developed, as has a simulation tool for the friction welding process in question.
At SPS the concept of 3-D printing of powder material components will be further pursued with other materials as this process compared to present compound production methods is likely to involve cost reductions and facilitate alternative design solutions.
MDT will apply the newly developed simulation tool not only in connection with alternative versions of a heavy duty valve spindle, but also other combustion chamber components which are expected to show creep under service conditions. The ability to produce a valve spindle with a hollow stem already is incorporated in a project with an active cooled valve spindle, while future friction welding design will benefit from the simulation tool developed by DTU.
As to the continued development of the HIP compound spindle design this will depend on the outcome of an evaluation of the necessary resources to solve the open issues, which most likely have to be supplied by MDT. Last but not least the future direction will depend on an evaluation of the competitiveness of the HIP compound solution compared to a recently introduced alternative and one other alternative execution, both based on conventional production methods.

Annex

[1] H. Hoeg and A. Lapina, "Exhaust valve for high temperatures", Minutes of meeting, Copenhagen 2015-11-10.

[2] H. Hoeg and A. Lapina, "Exhaust valve for high temperatures> meeting nr 5", Minutes of meeting, Copenhagen 2017-01-24.

[3] A. Nassour et al, “Creep properties of austenitic stainless-steel weld metals”, Journal of Materials Engineering and Performance, Vol. 10(6), December 2001, pp 693-698.

[4] A. Lapina et al, “Exhaust valve spindles for marine diesel engines manufactured by hot isostatic pressing”, Paper presented at the 12th International Conference on Hot Isostatic Pressing, Sydney, 2017.

[5] M. R. Sonne and J. H. Hattel, Thermal modelling of direct drive friction welding of 3Cr20Ni10W2 austenitic stainless steel rods applying a thermo-pseudo-mechanical (TPM) model, submitted to Journal of Advanced Manufacturing Technology

[6] M. R. Sonne and J. H. Hattel, Thermomechanical modelling of direct-drive friction welding applying a thermal pseudo mechanical model for the generation of heat, the International Conference on Tribology in Manufacturing Processes and Joining by Plastic Deformation 2018 (in Helsingør)